

1 Title: Ecology and genomic background shape the probability of
2 parallel adaptation to climate

3 Short title: Adaptation repeats itself probabilistically

4 Samridhi Chaturvedi^{1,2,3}, Zachariah Gompert³, Jeffrey L. Feder⁴, Owen G. Osborne⁵, Moritz
5 Muschick^{6,7}, Rudiger Riesch⁸, Víctor Soria-Carrasco⁹ and Patrik Nosil^{3,10}

6
7 ¹Department of Integrative Biology, University of California, Berkeley, California 94703 USA

8 ²Department of Organismic and Evolutionary Biology, Harvard University, Cambridge, Massachusetts,
9 02138, USA

10 ³Department of Biology and Ecology Center, Utah State University, Logan, Utah 84322, USA

11 ⁴Department of Biological Sciences, University of Notre Dame, Notre Dame, Indiana 46556, USA

12 ⁵Molecular Ecology and Evolution Bangor, Environment Centre Wales, School of Natural Sciences,
13 Bangor University, Bangor, LL57 2UW, UK

14 ⁶Aquatic Ecology & Evolution, Institute of Ecology and Evolution, University of Bern, CH-3012,
15 Switzerland

16 ⁷Department of Fish Ecology & Evolution, Eawag, Swiss Federal Institute for Aquatic Science
17 and Technology, CH-6047, Kastanienbaum, Switzerland

18 ⁸Department of Biological Sciences, Royal Holloway University of London, Egham, TW20 9EX, UK

19 ⁹The John Innes Center, Norwich Research Park, Norwich, NR4 7UH, UK

20 ¹⁰CEFE, Univ Montpellier, CNRS, EPHE, IRD, Univ Paul Valéry Montpellier 3, Montpellier, France

21 **ABSTRACT**

22
23 Evolution can repeat itself, resulting in parallel adaptations in independent lineages occupying
24 similar environments. Moreover, parallel evolution sometimes, but not always, uses the same
25 genes. Two main hypotheses have been put forth to explain the probability and extent of parallel
26 evolution. First, parallel evolution is more likely when shared ecologies result in similar patterns
27 of natural selection in different taxa. Second, parallelism is more likely when genomes are
28 similar, because of shared standing variation and similar mutational effects in closely related
29 genomes. Here we combine ecological, genomic, experimental and phenotypic data with
30 randomization tests and Bayesian modeling to quantify the degree of parallelism and study its
31 relationship with ecology and genetics. Our results show that the probability of parallel
32 adaptation to climate among species of *Timema* stick insects is shaped collectively by shared

33 ecology and genomic background. Specifically, the probability of genetic parallelism decays
34 with divergence in climatic (i.e., ecological) conditions and genomic similarity. Moreover, we
35 find that climate-associated loci are likely subject to selection in a field experiment, overlap with
36 genetic regions associated with cuticular hydrocarbon traits, and are not strongly shaped by
37 introgression between species. Our findings shed light on when evolution is most expected to
38 repeat itself.

39 INTRODUCTION

40 To what extent is evolution predictable and repeatable? This was the question posed by Stephen
41 J. Gould's famous thought experiment on whether repeatedly 'replaying the tape of life' would
42 yield similar evolutionary outcomes (Gould 1990). Gould considered similar outcomes unlikely,
43 due to chance events and historical contingency in evolution, and this thought experiment helped
44 launch decades of research on the repeatability of evolution. Indeed, the answer to this question
45 is important because it is central to understanding the processes shaping biological
46 diversification (Stern and Orgogozo 2009; Langerhans 2010; Losos 2011). For example,
47 instances of repeated or parallel evolution in response to similar environmental pressures can
48 provide evidence of evolution by natural selection. In contrast, idiosyncratic outcomes can
49 support a role for chance or contingency in evolution and indicate constraints on the power of
50 selection. The predictability of evolution also has practical implications, for example for
51 forecasting organismal responses to natural and human-induced environmental change
52 (Waldvogel et al. 2020), the planning of plant and animal breeding programs, and the design of
53 medicines and strategies to combat the spread of disease (Lieberman et al. 2011).

54 It is now known that evolution can repeat itself but does not always do so (Grant and Grant 2002;
55 Bolnick et al. 2018). Moreover, parallelism has been documented at the genetic level, with
56 striking cases of parallel evolution at single genes of major effect, at both the within- and among-
57 species level. For example, the *Ectodysplasin* gene controlling body armor has repeatedly been
58 used by numerous populations of stickleback fish during freshwater adaptation (Colosimo et al.
59 2005). Likewise, the *Agouti* and *McIR* genes control coloration in diverse organisms (Kingsley
60 et al. 2009; Manceau et al. 2010; Linnen et al. 2013). Beyond case studies, meta-analyses have
61 shown that parallel phenotypic evolution often involves the same genomic region (Elmer and

62 Meyer 2011; Stern 2013; Greenway et al. 2020). In contrast to these studies of major genes,
63 parallelism is less understood when evolution involves many genes of smaller effect, although
64 studies of genome-wide variation are beginning to fill this gap (Barrett and Schluter 2008;
65 Yeaman 2015; Yeaman et al. 2016; Papadopoulos et al. 2021). However, as noted, evolution is not
66 always parallel. Indeed, the probability of parallelism declines with the time since divergence
67 between taxa (Arendt and Reznick 2008; Conte et al. 2012). Although this decline is fairly
68 established, its likely causes are potentially complex (i.e., time itself is not the causal agent
69 controlling parallelism; rather factors such as ecology and genetics are likely involved, as
70 outlined below and as we test here) and remain poorly resolved, particularly beyond
71 experimental evolution experiments in microbes (i.e., for multicellular organisms in the wild)
72 (Bailey, Rodrigue, and Kassen 2015; Lenski 2017). Our goal here is to elucidate the factors
73 shaping the probability of parallel evolution in the wild, focusing on the proportion of the
74 genome undergoing parallel evolution.

75 In this context, two general hypotheses have been put forth, which are not mutually exclusive.
76 First, parallel evolution is more likely when shared ecologies result in similar patterns of natural
77 selection in different taxa (the ‘shared ecology’ hypothesis) (Roda et al. 2013; Stuart et al. 2017;
78 Morales et al. 2019). Shared aspects of environmental variation can decline with time since
79 divergence, for example as species come to occupy different geographic areas, thus reducing
80 parallelism (Manousaki et al. 2013; Rennison et al. 2020; Morales et al. 2019). Second,
81 parallelism is expected to be more likely when genomes are similar, because pools of standing
82 variation, the mutations which arise, and mutational effects are more similar in closely-related
83 genomes (the ‘shared genetics’ hypothesis; we use this term to also encompass the role of gene
84 regulation and development) (Schluter et al. 2004; Stern 2013; Roesti et al. 2014). Interactions
85 between genes (i.e., epistasis) might be particularly important here, because the effects of new
86 mutations are then dependent on the mutations which preceded them. Because new mutations are
87 most likely to have different effects in divergent genomes, gene reuse is reduced between
88 divergent genomes.

89 Both ecological and genetic similarity are expected to decline with time and there is support for
90 both hypotheses in studies of microbial experimental evolution (Matos et al. 2015; Good et al.
91 2017), protein evolution (Storz 2016), and comparative phylogenetic analyses (Conte et al. 2012;

92 Kohler et al. 2015). However, few studies have simultaneously examined ecology and genetics
93 such that the relative contribution of the two hypotheses remains unclear. Parsing these
94 contributions is important because it is required to test the fundamental roles of selection (i.e.,
95 shared ecology) and constraint (i.e., shared genetics) in evolution (Haldane 1990; Gompel and
96 Carroll 2003; Schlüter et al. 2004; Orgogozo 2015; Blount, Lenski, and Losos 2018). Here we
97 combine ecological data, genomic analyses, a field experiment, and genetic mapping to ascertain
98 the genetic basis and causes of parallel adaptation to climate, thus testing the shared ecology and
99 genetics hypotheses. In other words, rather than focusing on time *per se*, we conduct analyses
100 that jointly consider the degree of ecological and genetic divergence between taxa, to parse their
101 relative contributions to explaining the degree of parallel evolution observed.

102 Our study system is the wingless, univoltine, herbivorous stick insects in the genus *Timema*,
103 many species of which are found in California, USA (Nosil 2007). These insects are perhaps
104 best-studied for their cryptic colours and colour-patterns, which are controlled by the same
105 general genetic region in all species studied to date (i.e., the major locus named *Mel-Stripe*)
106 (Lindtke et al. 2017; Villoutreix et al. 2020). *Timema* colouration thus provides a striking
107 example of highly parallel evolution at the level of a single, non-recombining major locus.
108 However, adaptation often involves many genes, including those with alleles of minor effect
109 (Barghi, Hermission, and Schlötterer 2020; Rockman 2012), where the probability of parallel
110 genetic evolution is less clear (Yeaman 2015). In this context, we study here a novel ecological
111 dimension in *Timema*, namely climate, motivated by the facts that climate adaptation may be
112 polygenic, and that the genus *Timema* is distributed across a wide range of habitats in California.
113 For example, the used habitats range from sea-level to thousands of meters of elevation in
114 mountainous regions, and from arid semi-deserts near the Mexican border to wetter, evergreen
115 forests in northern California (Law and Crespi 2002). Moreover, there is climatic variation both
116 within and among species, with several species being distributed along elevational gradients
117 (ranging from 10 ft to ~2800 ft) (Nosil et al. 2020).

118 This variation allows us to find climate-associated genetic regions within species for multiple
119 species that span a range of divergence times from millions to tens of millions of years (here,
120 generations). Moreover, we thus quantify the proportion of the genome that exhibits parallel
121 association to climate across species, to test the shared ecology and shared genetics hypotheses.

122 In turn, we use a field experiment and genetic mapping to bolster the evidence that climate-
123 associated loci are likely subject to selection and to identify some of the traits involved. Finally,
124 we conduct genomic analyses that test the role of evolutionary history, specifically gene flow
125 and introgression, in observed parallelism. The collective results yield a comprehensive
126 evaluation of parallel evolution at the genome-wide level, in the context of an environmental
127 pressure of high current interest (i.e., climate), and in a system where comparison can be made to
128 parallelism seen at a single, major locus (i.e., *Mel-Stripe*). In contrast to accumulating examples
129 of adaptive introgression in birds, plants, fish, insects, and other animals (Heliconius Genome
130 Consortium 2012; Roesti et al. 2014; Henning and Meyer 2014; Bay, Taylor, and Schluter 2019;
131 Marburger et al. 2019; Giska et al. 2019; Menon et al. 2021), we find that introgression is
132 unlikely to play a key role in *Timema*. Thus, parallelism in *Timema* is likely most strongly
133 influenced by balancing selection on standing variation and the emergence of new mutations,
134 suggesting a diversity of mechanisms for repeated evolution.

135 RESULTS

136 **Climatic variation within- and among-species.** We studied eight *Timema* species across 53
137 geographic localities ($n = 1420$ individuals). Due to high correlations among the 22 studied
138 climate variables, we performed an ordination analysis using principal component analysis
139 (PCA) of the 22 climate variables for all populations included in the study (see Figure 2A for
140 species range map). This revealed that most of the variation in climate variables was explained
141 by the first three principal components (PC) (Total = 92.2%, PC1 = 51.7%, PC2 = 24.4% and
142 PC3 = 16.1%), which we hereafter focus on and refer to as PC1, PC2, and PC3 (Table S2 for PC
143 loadings, Figure S1).

144 The PC loadings allowed interpretation of the main factors contributing to each PC (variables
145 with PC loadings > 0.25 were considered top variables). For PC1, the top four variables were (i)
146 elevation (Ele), (ii) precipitation of warmest quarter (BIO18), (iii) precipitation of driest quarter
147 (BIO17), and (iv) precipitation of driest month (BIO14) (Figure S1A, Figure S1C, Table S2).
148 Therefore, PC1 is a general axis of elevation and precipitation variation, with high values
149 representing wet localities at high elevation (and conversely, low values representing low-
150 elevation dry sites). For PC2, the top four explanatory variables were (i) mean temperature of

151 warmest quarter (BIO10), (ii) maximum temperature of warmest quarter (BIO5), (iii) mean
152 temperature of driest quarter (BIO9), and (iv) annual mean temperature (BIO1) (Figure S1A,
153 Figure S1B, Table S2). Therefore, PC2 is a general axis of temperature variation, with high
154 loadings representing localities experiencing high temperatures. Lastly, for PC3, the top four
155 explanatory variables were: (i) precipitation of wettest quarter (BIO16), (ii) precipitation of
156 wettest month (BIO13), (iii) precipitation of coldest quarter (BIO19), and (iv) mean temperature
157 of driest month (BIO9) (Figure S1B, Figure S1C, Table S2). Therefore, PC3 is an axis of
158 contrasting variation in precipitation and temperature, with high values representing localities
159 closer to the coast experiencing greater temperature and precipitation fluctuations.

160 Overall, precipitation variables consistently loaded strongly on the first 3 PCs, followed by
161 temperature and elevation. One way ANOVA revealed significant between-species variation for
162 all three PCs (PC1: F value 104.5, *P*-value = < 0.0001; PC2: F value 104.5, *P*-value = < 0.001;
163 PC2: F value 6.803, *P*-value = < 0.0001; PC3: F value 28.07, *P*-value = < 0.0001). We also
164 detected clear within-species variation (range of median PC scores values across the eight
165 species were -3 and 5.8 for PC1, -2.5 to 6.5 for PC2, and -1.6 to 3.5 for PC3; Figure 2C-D). We
166 draw attention particularly now to PC3, as several of the most compelling results that follow
167 concern this PC. We describe a summary of our analyses in Figure 1.

168 **Identifying climate-associated genomic regions within species**

169 We first identified the genomic regions most strongly associated with climatic variation within
170 each of the eight species. To do so, we analyzed single nucleotide polymorphisms (SNPs)
171 obtained through previous genotyping-by-sequencing of natural populations (Riesch et al. 2017)
172 to quantify the number of genetic regions associated with climatic variation within each *Timema*
173 species. Because individual SNPs and their numbers differ among species, we focus on 100 kilo
174 base (Kb) SNP windows to allow eventual comparisons among species ($n = 9487$ windows in
175 each species, across the eight study species).

176 For each species, we quantified SNP-climate associations for each of the three climate PCs using
177 BayPass (version 1.2). This software controls for background population structure and generates
178 Bayes Factors (BF), which indicate the evidence for an association of each SNP with an
179 environmental variable (in our case, a PC axis). For each PC, we ran four Monte Carlo Markov

180 Chain (MCMC) simulations, each with a 20,000-iteration burn-in and 500 sampling iterations
181 with a thinning interval of 100. We used the default option of importance sampling to calculate
182 the regression coefficient (βi), which describes the association of each SNP with climate PC
183 scores. These coefficients were then used to calculate Bayes Factors, which were used to
184 compare the marginal likelihoods of models with non-zero versus zero values of βi . For each
185 species, we then calculated the median of logarithmic BF values for all the SNPs in the 100 kb
186 window and identified top SNP windows as those with medians in the top 10% empirical
187 quantile (“climate-associated SNP windows” hereafter). By using this approach, we incorporated
188 multiple loci spread across the genome in our analyses and avoided focusing on a single region
189 of the genome. Additionally, we expected this range of quantile to be enriched for loci truly
190 involved in climate adaptation. Finally, this approach allowed us to make comparisons among
191 species in downstream analysis. In all species, the top climate-associated SNP windows were
192 widely distributed across the genome and found on all 13 linkage groups (LGs) (Figure 3, Figure
193 S2, Figure S3).

194 **Parallel evolution of climate-associated genomic regions across species**

195 We next quantified the extent to which climate-associated SNP windows were parallel (i.e., the
196 same) across the eight species of *Timema* that we studied. We did so by testing if such windows
197 exhibit excess overlap across species relative to that expected by chance. We used two related
198 approaches. First, we asked if climate-associated SNP windows exhibited excess overlap
199 between each pair of species (“pairwise-comparison”, Figure 1B). Second, we asked if climate-
200 associated SNP windows exhibited excess overlap among multiple species i.e., if the same SNP
201 windows show association with climate PCs between 3, 4, 5, 6, 7 or 8 species (“multi-species
202 comparison”, Figure 1B). To do so, we conducted randomisation tests to quantify excess overlap
203 of windows relative to expectations assuming that SNP-climate associations were independent
204 across species, for pairwise as well as multi-species comparisons (Figure 1A). As an example, an
205 x-fold enrichment of 2.0 in the parallelism analyses would indicate that the evidence for overlap
206 of climate-associated SNP windows for a given comparison was two times higher than expected
207 by chance (based on the mean of the null). For this, we focused on windows with the greatest
208 (top 10%) climate association in nature (for all three climate PCs.)

These analyses revealed compelling evidence for parallel climate-associated SNP windows across species. For pairwise comparisons, we detected significant excess overlap in climate-associated SNP windows for all three climate PCs for at least some species pairs (Figure 4A, Figure S4A, and Figure S5A). For example, we observed excess overlap between eight species pairs for PC1 (Figure S4B), one species pair for PC2 (Figure S5B), and five species pairs for PC3 (Figure 4B). The quantitative degree of excess overlap was somewhat variable. For example, for PC1, the overlap of climate-associated SNP windows among the seven species pairs that showed a significant excess of overlap ranged from an x-fold enrichment of ~1.3x for *T. knulli* and *T. poppensis* (observed = 36, expected = 27, x-fold enrichment = 1.31, *P*-value = 0.04) to a maximum x-fold enrichment of ~2x for *T. podura* and *T. chumash* (observed = 23, expected = 11, x-fold enrichment = 2.20, *P*-value = 0.01) (Figure S4A-B). For PC2, there was only one species pair, *T. bartmani* and *T. californicum*, which showed significant excess overlap of SNP windows with largest median Bayes factors (observed = 29, expected = 19, x-fold enrichment = 1.48, *P*-value <.01; Figure S5B). Lastly, for PC3, the overlap of climate-associated SNP windows among the five species pairs that showed a significant excess of overlap ranged from an x-fold enrichment of ~1.2x for *T. cristinae* and *T. landelsensis* (observed = 49, expected = 38, x-fold enrichment = 1.29, *P*-value = 0.03) to ~1.5x for *T. bartmani* and *T. cristinae* (observed = 27, expected = 17, x-fold enrichment = 1.53, *P*-value = 0.01) (Figure 4A-B).

Parallelism was also supported in analyses examining multi-species (i.e., beyond pairwise) comparisons. For PC1, there was significant excess overlap of SNP windows with largest median Bayes factors between three or more species ~2x more than expected by chance (observed = 60, expected = 26.77, x-fold enrichment = 2.25, *P*-value < 0.01; Figure S4C), for four or more species about ~3x more than expected by chance (observed = 4, expected = 1.03, x-fold enrichment = 3.87, *P*-value 0.02; Figure S4C). For PC2, there was significant excess overlap of SNP windows with largest median Bayes factors between three or more species about ~1.5x more than expected by chance (observed = 42, expected = 26.41, x-fold enrichment = 1.59, *P*-value <.01; Figure S5C), for four or more species about ~4x more than expected by chance (observed = 5, expected = 1.19, x-fold enrichment = 4.17, *P*-value = 0.007; Figure S5C). Lastly, for PC3 there was significant excess overlap of climate-associated SNP windows between three or more species ~1.6x more than expected by chance (observed = 43, expected = 26, x-fold enrichment = 1.63, *P*-value < 0.01; Figure 4C). This effect was even stronger for shared

240 windows among four or more species (observed = 5, expected = 1.10, x-fold enrichment = 4.53,
241 *P*-value = 0.006; Figure 5C). Similar results were observed for PC1 and PC2 (Figure S4C and
242 Figure S5C). After finding this evidence for parallelism, we turned to testing our core two
243 hypotheses, by quantifying the extent to which parallelism decays with ecological divergence,
244 genomic divergence, or both.

245 **Parallelism declines predictably with ecological and genomic divergence between species**

246 We next tested the shared ecology and shared genetics hypotheses for variation in the degree of
247 parallelism. Shared ecology would cause a higher degree of parallelism due to similar selective
248 pressures from similar environments. On the other hand, shared genetics would a higher degree
249 of parallelism due to higher probability of gene reuse. Here, we quantified parallelism as the
250 degree of excess overlap of climate-associated SNP windows relative to null expectations, for
251 pairwise comparisons (Figure 2B). We estimated ecological similarity between pairs of species
252 using climatic data and genetic similarity based on a previously published phylogeny. We then
253 fit Bayesian linear mixed models to explicitly compare models where the degree of parallelism is
254 determined by ecological similarity, genetic similarity, and both. Notably, this mixed model
255 approach accounts for the non-independence of pairwise distances (Gompert et al. 2014 for
256 details). Specifically, for each climatic PC variable, we modeled parallelism as the x-fold excess
257 in shared top climate-associated SNP windows (as described in the preceding section) as a
258 function of climatic distance which was calculated as the average difference in climate PC scores
259 between a given pair of species (hereafter referred to as ecology indicating “divergence in
260 ecology”), phylogenetic distance (hereafter referred to as genes indicating “divergence in
261 genetics”), or both. We tested the effect of both ecology and genetics on parallelism (Figure 5B,
262 Figure S6B, Figure S7B). The fit of the different models with or without ecology or genetics was
263 compared using deviance information criterion (DIC), which is a metric of predictive
264 performance.

265 Our analyses revealed evidence for effects of both ecology and genes on the probability of
266 parallelism, with results that varied among the climate PCs (Figure 5C-D for PC3, Figure S6C-D
267 for PC1, Figure S7C-D for PC2). For PC3, the full model (ecology and genes) was the best
268 model, with similar, negative effects on parallelism of divergence in ecology (standardized beta
269 = -0.47, 95% CI = -0.80 to -0.14) and divergence in genes (standardized beta = -0.55, 95% CI = -

270 0.87 to -0.21; Figure 5E; Table S3). For PC1, the genes-only model was the best model
271 (standardized beta = -0.55, 95% CI = -0.8 to -0.25; Figure S6E, Table S3). The second-best
272 model was the full model, but this included a positive rather than negative effect of ecological
273 distance on parallelism. Lastly, for PC2 the best model was a null model of no effect of genes or
274 ecology on parallelism (Figure S7E, Table S9). The results thus provide variable support for both
275 the shared ecology and shared genetics hypotheses, dependent on climate PC and strongest for
276 PC3. Having tested these hypotheses, we next tested for additional evidence, beyond parallelism,
277 that the climate-associated SNP windows have been affected by natural selection.

278 **Climate-associated regions exhibit elevation-dependent allele-frequency change in a field**
279 **experiment and co-vary with CHCs in *T. cristinae***

280 To potentially bolster the evidence that climate-associated SNP windows are enriched for genetic
281 variants experiencing natural selection, we next tested if such windows exhibited exceptional
282 patterns of allele-frequency change in a transplant-and-sequence field experiment and if they
283 overlap with regions associated with phenotypic variation in genetic mapping analyses. Here, an
284 x-fold enrichment of 2.0 in the CHC analysis would indicate that the evidence for SNP-CHC
285 associations in climate-associated SNP windows was two times higher than expected by chance
286 (based on the mean of the null, see below for details).

287 The transplant experiment measured 8-day survival and associated genome-wide allele frequency
288 change during this period in 500 *T. cristinae* transplanted to 10 experimental bushes comprising
289 two host plants and all occurring at a gradient of higher elevations than the source population for
290 the experiment. A previous analysis of this experiment documented evidence of selection
291 associated with elevation. Here, as a metric of possible elevation (environment)-dependent
292 selection, we calculated the Pearson correlation between transplant elevation and allele
293 frequency change caused by mortality during the experiment for each SNP. In this current
294 analysis, we found that 100 kb windows exhibiting patterns of allele frequency change most
295 strongly associated with elevation in the transplant experiment coincided modestly with climate-
296 associated SNP windows, but more than expected by chance. Specifically, when focusing on the
297 windows with the greatest (top 10%) correlation between change and elevation in the experiment
298 and with the greatest (top 10%) climate association in nature, windows associated with all three
299 climate PCs corresponded with those where change was most strongly associated with elevation

300 ~1.2-1.3 times more than expected under the null hypothesis of independence (constrained
301 randomization test controlling for SNP density within windows based on 1000 randomizations;
302 PC1: observed = 108 shared windows, $P = 0.005$; PC2: observed = 101 shared windows, $P =$
303 0.015; PC3: observed = 105, $P = 0.021$ windows) (Figure 6). Similar patterns were observed
304 where more extreme top percentiles were considered, and when using an unconstrained
305 randomization test (Table S4). These patterns are consistent with the hypothesis that multiple
306 genetic variants in these windows are subject to selection in nature.

307 For the CHC analyses, we considered three compound classes - pentacosanes, heptacosanes, and
308 nonacosanes - in males and in females (i.e., six CHC traits total). We found evidence of heritable
309 variation for each compound in both male and female *T. cristinae*, with 50.8% (male
310 nonacosanes) to 89.7% (female pentacosanes) of the variability in these traits explained by ~176
311 thousand sequenced SNPs in a mapping population (these values denote Bayesian point
312 estimates; these results are based on 602 *T. cristinae* from a single population, FHA) (see Table
313 S5 for details). We summarized the evidence that each 100 kb window included CHC-associated
314 SNPs by computing the mean posterior probability of association (i.e., the mean probability of a
315 non-zero genotype-phenotype association, also known as the posterior inclusion probability or
316 PIP) across SNPs in 100 kb windows (i.e., the same 100 kb windows used for summarizing SNP-
317 climate associations). Then, based on a randomization test, we found that for some CHC traits,
318 the average posterior inclusion probability for SNPs in the top climate-associated SNP windows
319 in *T. cristinae* was marginally but significantly greater than expected by chance. Specifically, the
320 average probability of SNPs being associated with female pentacosanes was ~1.05 times higher
321 than expected by chance for both the top 10% of PC2 and PC3 climate-associated SNP windows
322 (P -value = 0.009 for PC2 and P -value = 0.010 for PC3 based on 1000 permutations; Figure 5B,
323 Table S7 and S8). We also detected a marginally non-significant increase in the average
324 posterior inclusion probability for SNP associations with female nonacosanes in the top 10% of
325 PC3 climate-associated SNP windows (x-fold increase in mean inclusion probability = 1.03, P -
326 value = 0.051, 1000 permutations, Table S8). These results from CHCs support the hypothesis
327 that at least a subset of the top climate-associated SNP windows are associated with traits
328 involved in climatic adaptation in *Timema*. Thus, together with the results presented in the
329 previous paragraph, these results suggest a polygenic basis for climatic adaptation in *T. cristinae*
330 with at least a modest correspondence between our top climate-associated windows and the

331 actual loci involved in climate adaptation. With this evidence, we next turn to additional analyses
332 concerning the evolutionary history and mechanisms of parallelism, namely the potential role of
333 introgression between species in promoting parallelism.

334 **Introgression between species does not contribute strongly to parallel evolution**

335 We conducted two analyses, focused on different time scales, to ask if introgression and gene
336 flow between species promotes gene sharing and thus climate-associated parallel evolution. First,
337 we identified historical patterns of introgression using a population tree-based approach. Second,
338 we identified contemporary patterns of gene flow using an admixture model. Both these analyses
339 helped us to assess the degree of genetic independence in adaptation to climate within each
340 species.

341 To identify historical patterns of introgression, we used TREEMIX to generate a population tree
342 for all populations and species while allowing for historical admixture or gene flow among intra-
343 specific or inter-specific populations. For this analysis, we realigned GBS sequence data for all
344 1420 individuals included in this study to the *T. cristinae* genome. We then called and filtered
345 single nucleotide polymorphisms (SNPs) to identify final set of 8787 SNPs for this analysis. Our
346 results from TREEMIX yielded a population graph or bifurcating tree depicting relationships
347 between focal localities in this study. The best bifurcating tree explained 99.6% of the variation
348 in the population allele-frequency covariances. In this tree, *Timema* populations formed eight
349 major clades that grouped populations by species (Figure 5A). Adding migration edges to the
350 tree increased the variance explained by a negligible extent (Table S9), a logical result given that
351 the tree with no migration edges explained the overwhelming majority of the variation in the
352 data. These results are consistent with little to no introgression between species, a result reported
353 previously for analogous analyses that focused on only the *Mel-Stripe* locus (Villoutreix et al.
354 2020).

355 We further used the admixture model from ENTROPY (version 1.2) to infer contemporary gene
356 flow. This analysis was based on the full data set of 1420 individuals and species-specific SNPs
357 (see methods for details). Here we focused on admixture proportions for k=2, as we were
358 interested in the two nominal species and hybrids between them. Additionally, all our analyses
359 focused on pairs of species. We summarized patterns of population structure and admixture

360 across the sampled populations and individuals based on these admixture proportions and a
361 principal component analysis (PCA) of the genotypic data (Figure S8-S10). As previously
362 reported (Riesch et al. 2017; Villoutreix et al. 2020), we saw minimal evidence of contemporary
363 admixture between species. Together these results suggested that introgression and gene flow do
364 not strongly or regularly influence the dynamics of parallel adaptation to climate in these species.

365 CONCLUSION

366 We used GBS data from 1420 individuals across eight species, combined with other forms of
367 data, to show that adaptation to climate occurs in parallel across species but as a function of
368 the ecological and genomic divergence between species. Our results inform three fundamental
369 issues in biology, namely the repeatability of evolution, the effect of ecology and genetics on
370 parallelism, and the processes promoting parallelism. We treat these in turn.

371 Firstly, we show that evolution in response to climate occurs in parallel among eight species and
372 that parallelism likely involves multiple loci. These findings fill a gap in our knowledge of
373 parallel evolution because many studies, including past work in *Timema*, have mostly focused on
374 parallelism driven by single-genes or specific regions of the genome (Colosimo et al. 2005;
375 Kingsley et al. 2009; Villoutreix et al. 2020). These results agree with other cases of parallel or
376 convergent climate adaptation which are also driven by polygenic interactions, as for example
377 observed in plants (Yeaman et al. 2016; Walden, Lucek, and Willi 2020; Rose et al. 2018;
378 Blanco-Pastor et al. 2021). Our study demonstrates that repeatability of evolution can be driven
379 by numerous genetic paths, but the magnitude of repeatability can be highly variable, specifically
380 when considering inter-species comparisons.

381 Second, our results also show that parallelism decays with ecological and genetic divergence,
382 suggesting that both shared ecology and shared genetics can affect parallel evolution. Similar
383 ecological settings can exert similar selection pressures which drive parallel evolution in
384 populations inhabiting similar geographical niches even among species (Stuart et al. 2017). In
385 addition, genetic similarity could lead to access to the same standing genetic variation in closely
386 related taxa, which allows gene reuse in response to similar environmental pressures (Bohutínská
387 et al. 2021). Our study demonstrates that both these aspects can affect parallelism, with a perhaps
388 stronger or more consistent effect of genetics. This makes sense as ecological settings are

389 perhaps more complex compared to genetics and the ecological variation considered can be
390 context-dependent.

391 Third, our collective results inform how two core evolutionary processes, namely
392 introgression/gene flow and selection, might affect parallelism. For example, we show that
393 parallel evolution and adaptation to climate occurs despite limited or minimal gene flow among
394 and within species, wherein we show little to no introgression among our focal study species.
395 While introgression can facilitate parallel adaptation to similar environmental pressures by
396 providing novel genetic material (Heliconius Genome Consortium 2012; Roesti et al. 2014;
397 Henning and Meyer 2014; Bay, Taylor, and Schluter 2019; Marburger et al. 2019; Giska et al.
398 2019; Menon et al. 2021), a lack of introgression or gene flow demonstrates independent
399 instances of adaptation and the role of selection in driving parallel evolution (Zhang et al. 2021).
400 In summary, our study shows how local adaptation even among species with minimal gene flow
401 can occur and consequently be crucial for predicting evolution in response to rapidly changing
402 environments and climate. Furthermore, our results bolster evidence for selection beyond a
403 correlational genome scan because we found that the genomic regions which underlie parallelism
404 also showed marked allele-frequency change in an experiment and were associated with
405 ecologically relevant CHC traits. Thus, together these results suggest that allele reuse through
406 standing genetic variation, new mutations, and selection can be powerful drivers of local
407 adaptation.

408 **METHODS**

409 Below we describe details of all our methods and analyses, and we provide a graphic summary in
410 Figure 1 of the main text.

411 **Samples and DNA sequences from natural populations**

412 For this study, we analyzed genotyping-by-sequencing (GBS) data from 1420 *Timema* stick
413 insects from 53 localities from eight species: 6 *T. bartmani* populations ($N = 195$ individuals), 3
414 *T. californicum* populations ($N = 77$ individuals), 12 *T. chumash* populations ($N = 358$
415 individuals), 6 *T. cristinae* populations ($N = 205$ individuals), 5 *T. knulli* populations ($N = 89$
416 individuals), 4 *T. landenlsensis* populations ($N = 125$ individuals), 12 *T. podura* populations ($N =$
417 12 individuals) and 5 *T. poppensis* populations ($N = 116$ individuals) (Table S1). GBS data for

418 this study has been previously published in a study of speciation continuum in *Timema* (Riesch
419 et al. 2017) (also see data availability for more details). The genomic data in the transplant
420 experiment and used for genetic mapping of cuticular hydrocarbons is independent from these
421 data and is described in detail below.

422 **Sequence alignment and variant calling**

423 To incorporate variants typed for individuals of each species, we built a consensus reference
424 sequence for each species (similar to (Comeault et al. 2016; Villoutreix et al. 2020)). To do this,
425 we first aligned all reads from all our samples to the *T. cristinae* reference genome (draft version
426 0.3) using the MEM algorithm of BWA (Version: 0.7.17-r1188) (Riesch et al. 2017). We ran
427 BWA MEM with a minimum seed length of 15 (-k), internal seeds of longer than 20 bp, and only
428 output alignments with a quality score of ≥ 30 (-T). We then used SAMTOOLS (version 1.5) to
429 view, sort and index the alignments (Li et al. 2009). We called variants using SAMTOOLS and
430 BCFTOOLS (version 1.6) (Li et al. 2009; Danecek et al. 2021). For variant calling, we used the
431 mapping quality adjustment of 50 (-C), skipped alignments with mapping quality 0, skipped
432 bases with base quality 13, and ignored insertion-deletion polymorphisms. We then set the prior
433 on single nucleotide polymorphisms (SNPs) to 0.001 (-P) and called SNPs when the posterior
434 probability that the nucleotide was invariant was 0.01 (-p). We then performed two rounds of
435 filtering to retain final sets of SNPs. In the first round, we filtered the initial set of SNPs to retain
436 only those with sequence data for at least 80% of the individuals, a mean sequence depth of two
437 per individual, at least four reads of the alternative allele, a minimum quality score of 30, a
438 minimum (overall) minor allele frequency of at least 5%, and no more than 0.01% of the reads in
439 the reverse orientation. In the second round of filtering, we removed SNPs with excessive
440 coverage (2 standard deviations above the mean) or that were tightly clustered (within 5 base
441 pairs (bp) of each other) and removed variants with poor alignments. This left us with the
442 following number of SNPs for each species: 10,036 SNPs for *T. bartmani*, 14,955 SNPs for *T.*
443 *californicum*, 20,478 SNPs for *T. chumash*, 3,43,746 SNPs for *T. cristinae*, 25,835 SNPs for *T.*
444 *knalli*, 21,314 SNPs for *T. landelsensis*, 21,986 SNPs for *T. podura*, and 18,237 SNPs for *T.*
445 *poppensis*.

446 We used these filtered variants for each species to construct consensus reference sequences for
447 each species using the CONSENSUS algorithm of BCFTOOLS (version 1.6) (Danecek et al.

448 2021). We then used the consensus reference of each species to redo alignments for GBS
449 sequences of individuals for each species separately. Following this, we repeated variant calling
450 and two rounds of variant filtering as described above. This left us with the following number of
451 SNPs for each species: 3074 SNPs for *T. bartmani*, 7858 SNPs for *T. californicum*, 4172 SNPs
452 for *T. chumash*, 1,96,252 SNPs for *T. cristinae*, 11,139 SNPs for *T. knulli*, 8548 SNPs for *T.*
453 *landelsensis*, 6000 SNPs for *T. podura*, and 7157 SNPs for *T. poppensis*. We used this second set
454 of SNPs noted directly above for all downstream analyses.

455 **Climate variables and identifying SNP by climate associations in nature**

456 We used 22 climate layers values associated with our 53 study localities (Table S2), which were
457 extracted from the WorldClim database version 1.4
458 (<https://www.worldclim.org/data/v1.4/worldclim14.html>; climate data for 1960-1990). Since the
459 first three PC scores explained the overwhelming majority (92.4%) of variation in the climate
460 variables (Figure 2B, Table S2, Figure S1), we used these three PCs to study genomic
461 associations with climate in all further analyses.

462 We used BayPass version 2.1 (Gautier 2015) to identify genomic regions associated with the
463 three sets of PC scores for the climate variables. The BayPass software controls for background
464 population structure and is based on the BAYENV method introduced by Gunther and Coop
465 (Günther and Coop 2013). We ran this program separately for each species and for each PC
466 (eight species by three PCs). We treated each PCs scores as the environmental covariate and ran
467 the standard covariate model. For each data set, we ran four Monte Carlo Markov Chain
468 (MCMC) simulations, each with a 20,000-iteration burn-in and 500 sampling iterations with a
469 thinning interval of 100. We used the default option of importance sampling to calculate the
470 regression coefficient (β_i), which describes the association of each SNP with climate PC scores.
471 These coefficients were then used to calculate Bayes Factors which were used to compare the
472 marginal likelihoods of models with non-zero versus zero values of β_i . Finally, since we had
473 different number of focal SNPs for each species, we calculated median of logarithmic Bayes
474 Factors for 100 kilobase (kb) non-overlapping SNP windows (i.e., the same windows were used
475 in every species, facilitating comparisons among them). Our downstream analyses described
476 below focus on these windows. We delimited climate-associated SNP windows as those with

477 greatest association with the three climate PCs, specifically as the windows in the top 10%
478 quantile. We refer to such windows as “climate-associated SNP windows” hereafter.

479 **Quantifying parallel genomic associations with climate across species**

480 We quantified parallel genomic associations with climate across species (using the results
481 described above from BayPass) and used randomization tests to measure the extent to which the
482 observed parallelism exceeded that expected by chance. We report this excess as ‘x-fold’
483 enrichments, relative to null expectations, also reporting associated *P*-values for statistical
484 significance.

485 We first tested for excess overlap of climate-associated SNP windows between pairs of species
486 (“pairwise comparisons”), for each of the three climate PCs. To do this, we used randomization
487 tests (10,000 randomizations per test) to generate null expectations for the proportion of top
488 climate-associated SNP windows shared between a given pair of species and tested whether this
489 was significantly more than expected by chance (x-fold enrichments and *P*-values). As an
490 example, an x-fold enrichment of 2.0 would indicate that twice as many climate-associated SNP
491 windows showed overlap between a species pair than was expected by chance (based on the
492 mean of the null). We then quantified overlap in climate-associated SNP windows between
493 multiple species (“multi-species comparisons”) i.e., we tested if similar SNP windows show
494 association with climate PCs between 2, 3, 4, 5, 6 or 8 species. We did this by using similar
495 randomization tests as for pairwise-comparisons, to generate x-fold enrichments and *P*-values.

496 **Testing the shared ecology and shared genetics hypotheses**

497 We tested the contribution of shared ecology versus shared genetics to the observed degree of
498 parallelism. We expect both shared ecology and genetics to have an effect on the probability of
499 parallelism. To do so, we fit Bayesian linear mixed models to explicitly compare models where
500 parallelism is determined by ecological similarity, genetic similarity, or both. This Bayesian
501 regression analysis is based on the mixed model framework proposed by (Clarke, Rothery, and
502 Raybould 2002) and extended by (Gompert, Lucas, et al. 2014). Our method accounts for the
503 correlated error structure inherent in pairwise covariates and response variables (e.g., ecological
504 or genetic distances). In this analysis, our response variable was the x-fold excess in shared top
505 climate-associated SNP windows for a given PC (we did analyses separately for each climate

506 PC). Our independent variables were ecological and genetic distances, estimated as follows.
507 Climatic (i.e., ecological) distance was calculated as pairwise absolute mean difference of PC
508 scores of each species. We calculated genetic (i.e., phylogenetic) distances based on the
509 previously published phylogeny described in Riesch et al. 2017. Briefly, we used the data from
510 this previous phylogeny constructed using Bayesian phylogenetic inference with BEAST
511 (version 2.1.387) for 11 *Timema* species based on GBS data of curated dataset of 19,556 single-
512 nucleotide variants. For our current study, we used pairwise phylogenetic distances for the eight
513 *Timema* species as our metrics of genetic distances for this analysis. All variables were
514 standardized (given mean 0 and standard deviation of 1) before analysis.

515 We then considered four alternative models: (i) a null model without covariates, (ii) a model
516 including only phylogenetic distance, (iii) a model with only climatic distance, and (iv) a model
517 with both climate and phylogenetic distance. We fit the models in R using the rjags (version 4.8)
518 interface with Jags (version 4.3.0). We used minimally informative priors for the regression
519 coefficients (i.e., normal with $\mu = 0$ and precision $\tau = 0.001$) and for the population random
520 effects and residual errors, all gamma (1, 0.01). Deviance information criterion was used for
521 model comparison. Parameter estimates and DIC estimates were obtained via MCMC. For each
522 analysis and model, we ran three chains each comprising 10,000 sampling iterations, a 2000-
523 iteration burn-in, and a thinning interval of 5.

524 **Overlap of climate-associated SNP windows with genetic regions showing elevation-
525 associated change in a field experiment**

526 We quantified overlap between climate-associated SNP windows and windows that exhibited
527 elevation-dependent allele-frequency change in a previously published release-recapture field
528 experiment. We then tested if this overlap was greater than expected by chance. Full details of
529 the experiment can be found in the original publications (Gompert, Comeault, et al. 2014; Nosil
530 et al. 2018) but those relevant for the current study are as follows. The experiment involved
531 releasing 500 *T. cristinae* (from which a tissue sample was taken) onto 10 experimental bushes
532 (five blocks, each with one plant of *Adenostoma fasciculatum* and one of *Ceanothus spinosus*).
533 Survivors were recaptured eight days later. Whole-genome sequence data, which we analyze
534 here, was obtained from 491 of the 500 stick insects (Nosil et al. 2018).

535 For the current study, we estimated allele frequencies in the released and recaptured stick insects
536 at the 6,175,495 bi-allelic SNPs identified by Nosil et al. 2018. This was done using an
537 expectation-maximization (EM) algorithm as implemented in the program estpEM (version 0.1)
538 with tolerance of 0.001 and a maximum of 50 EM iterations (Soria-Carrasco et al. 2014). We
539 then used these estimates to compute allele-frequency change between the start and end of the
540 experiment. Then, for each SNP we calculated the Pearson correlation between allele frequency
541 change and the elevation at each of the ten transplant sites. Finally, we determined the average
542 correlation between change and elevation for the 100 kb windows across the genome. Windows
543 with fewer than four SNPs were ignored. These steps were done using R (version 3.4).

544 We then calculated the number of 100kb windows that were among the top 10% for both
545 elevation-dependent change during the experiment (highest average absolute correlation) and for
546 climate-association (highest average Bayes factor for each climate PC). We used a constrained
547 randomization procedure to generate null expectations for such concordance between change and
548 climate-association windows, using a separate randomization for each PC. Specifically, we
549 randomized mean change metrics across windows, but only among windows with similar SNP
550 densities (10 equally sized bins were used for this). This was done because we observed a
551 positive correlation between SNP density and mean change-elevation correlations per window
552 (Pearson $R = 0.069$, 95% CI = 0.047-0.091, $P < 0.001$), and we wanted to control for this. Null
553 distributions and P -values were based on 1000 randomizations and are reported for each climate
554 PC.

555 **Overlap of climate-associated SNP windows with genetic regions associated with cuticular
556 hydrocarbon variation**

557 Our next set of analyses concern climate-associated SNP windows and genomic regions
558 associated with cuticular hydrocarbon (CHC) variation. The logic here is that CHCs tend to play
559 a role in desiccation tolerance and climatic adaptation in insects (e.g., (Rajpurohit et al. 2017)),
560 such that genetic regions associated with climate versus CHCs might overlap. We thus
561 specifically quantified the extent to which climate-associated SNP windows overlapped with
562 windows harbouring SNPs associated with CHCs, and whether this overlap was greater than
563 expected by chance. The CHC data were originally described and analyzed by Riesch et al.
564 (2017). Specifically, for each insect we had quantified the proportional abundance of 26 different

565 mono- and di-methylated CHCs, which comprised eight pentacosanes, eight heptacosanes and
566 ten nonacosanes, and then applied log-contrasts. For the current dataset, we used those values to
567 calculate the proportional abundance of the sum of all pentacosanes, the sum of all heptacosanes
568 and the sum of all nonacosanes (henceforth: pentacosanes, heptacosanes and nonacosanes).
569 Therefore, the six CHC traits considered were pentacosanes, heptacosanes, and nonacosanes in
570 males and females (i.e., three molecule types in each of two sexes).

571 Here, we first re-aligned the GBS data from Riesch et al. (2017) to the current (i.e., more recent
572 and less fragmented) *T. cristinae* genome (draft version 0.3). This included GBS data from 395
573 male and 195 female *T. cristinae* all collected from a single population (FHA), and all of which
574 for CHC data was also collected. These data were aligned to the genome using the BWA ALN
575 algorithm (version 0.7.17-r1188) (Li 2013). We allowed for 5 miss-matches total, and not more
576 than 2 miss-matches in the first 20 bp. Only reads with a mapping quality greater than 10 were
577 retained. We then compressed, sorted and indexed the alignments with SAMTOOLS and
578 BCFTOOLS (version 1.2) (Li et al. 2009; Danecek et al. 2021). Next, we used SAMTOOLS and
579 BCFTOOLS to identify SNPs and calculate genotype likelihoods. For this, we used the
580 recommended mapping quality adjustment (-C 50), only considered alignments with mapping
581 qualities of 20 or more and SNPs with base qualities of 30 or more, and only called variants
582 when the posterior probability that locus was invariant was less than 0.01 given a prior mutation
583 rate parameter of 0.001. We then used custom perl scripts to filter out variants with a mean
584 coverage of less than 2x, fewer than 10 non-reference reads total, mapping quality less than 30,
585 minor allele frequency less than ~0.005, more than 1% of reads in the reverse orientation (with
586 our GBS method, all reads should have the same orientation), missing data (no reads) for more
587 than 20% of individuals, SNPs with more than two alleles, and SNPs with coverage exceeding
588 three standard deviations above the mean. Finally, we obtained Bayesian point estimates
589 (posterior means) of genotypes for each locus and individual based on the genotype likelihoods
590 and used the estimated allele frequencies to parameterize a binomial prior.

591 We then conducted genetic mapping of CHC variation using a polygenic genome-wide
592 association (GWA) mapping approach, that controls for linkage disequilibrium among SNPs and
593 background population structure as detailed below. We specifically fit Bayesian sparse linear
594 mixed models (BSLMMs) to determine the contribution of additive genetic variation (as

595 captured by our collective SNP data set) to each of six CHC traits, and to determine the
596 probability of association (posterior inclusion probability, PIP) of each individual SNP with each
597 trait (this PIP value is computed from, i.e., equal to, the proportion of MCMC samples that
598 included each SNP in the polygenic regression model). We fit this model using gemma (version
599 0.95a) (Zhou, Carbonetto, and Stephens 2013), a polygenic GWA mapping method that fits a
600 single model with all SNPs while accounting for uncertainty and redundancy in genotype-
601 phenotype associations, for example by controlling for linkage disequilibrium among SNPs, and
602 background polygenic effects. The latter is inferred based on a kinship matrix derived from the
603 collective SNPs, which also serves to control for population structure when estimating effects for
604 individual SNPs. Models were fit using MCMC, with each mapping exercise involving 10
605 independent chains each comprising 1 million sampling iterations and a 200,000-iteration burn-
606 in.

607 Based on these analyses, we then computed the mean PIP (i.e., probability of a genotype-
608 phenotype association) across all SNPs in 100 kb windows for each of the six CHC traits. Then,
609 we asked whether the average association with CHCs (averaged over windows) was higher for
610 the climate-associated SNP windows than expected by chance. Randomizations (1000) were
611 used to generate a null distribution. Specifically, mean posterior probabilities for SNP-CHC
612 associations were permuted across 1000 kb windows and the number windows in the top 10%
613 for climate association and (permuted) CHC posterior inclusion probabilities was determined.
614 Note that we conducted this test independently for each of the six CHC traits and each of the
615 three climate PCs. We then examined the combination of these results to assess the total
616 evidence that SNP windows associated with climate adaptation are enriched for those regions of
617 the genome possibly affecting CHC variation.

618 **Testing for introgression and quantifying population structure**

619 We quantified both historical and contemporary gene flow patterns, respectively as follows. For
620 identifying historical introgression, we used TREEMIX (version 1.13) (Pickrell and Pritchard
621 2012) to construct a population-based phylogeny to identify historical admixture or gene flow
622 among our 53 focal populations. This differed from previous TREEMIX analysis done for
623 *Timema* species where we used the data only from the *Mel-Stripe* locus (Villoutreix et al. 2020).
624 For the analysis in our study here, we re-aligned the GBS sequences for 1420 individuals (across

53 populations) included in this study to the *T. cristinae* genome (draft version 0.3). We did this by using the MEM algorithm from BWA (version 0.7.17-r1188). We ran BWA MEM with a minimum seed length of 15, internal seeds of longer than 20 bp, and only output alignments with a quality score ≥ 30 . We then used SAMTOOLS (version 1.6) to compress, sort and index the alignments (Li et al. 2009). We then identified SNPs using SAMTOOLS and BCFTOOLS (version 1.6). For variant calling, we used a mapping quality of 50, skipped alignments with mapping quality lower than < 20, skipped bases with base quality < 15, and ignored insertion-deletion polymorphisms. We set the prior on SNPs to 0.001 and called SNPs when the posterior probability that the nucleotide was invariant was ≤ 0.01 . After we got the initial set of variants, we filtered them to retain only those SNPs with sequence data for at least 80% individuals, a mean sequence depth of two per individual, at least 4 reads of the alternative allele, a minimum quality score of 30, a minimum overall minor allele frequency of at least 0.005, and no more than 1% of the reads in the reverse orientation (this is an expectation for our GBS method). We further removed SNPs with excessive coverage (3 standard deviations above the mean) or that were tightly clustered (within 3 bp of each other), as these could be poor alignments (e.g., reads from multiple paralogs mapping to the same region of the genome). This left us with 8787 SNPs for this analysis. We used these variants to run TREEMIX to fit trees allowing 0-9 admixture events and calculate the proportion of variance in allele frequency variances explained by the population tree with the varying numbers of admixture events. This way we could determine the extent to which individual admixture events improved model fit.

For estimating contemporary gene flow, we implemented the admixture model from ENTROPY (version 1.2) (Gompert, Lucas, et al. 2014). This analysis yielded similar results as previously reported using the same model (Riesch et al. 2017). From ENTROPY, we obtained Bayesian estimates of genotypes and admixture proportions. This analysis was performed separately for each species- and species-specific set of SNPs. We did this to identify contemporary gene flow within species to understand if gene flow could affect parallelism in response to climate. The admixture model in ENTROPY is similar to that in STRUCTURE (Pritchard, Stephens, and Donnelly 2000) but differs by accounting for uncertainty in genotypes arising from finite sequence coverage and sequence errors, and by allowing simultaneous estimation of genotypes and admixture proportions. For each species, we fit the model with $k \in \{2 \dots 5\}$ source

655 populations. For each value of k, we ran three MCMC chains, each with 8000 iterations, a burn-
656 in of 5000 iterations and a thinning interval of 3. We used assignments from a discriminant
657 analysis of principal components to initialize the MCMC algorithm; this speeds convergence to
658 the posterior and avoids label switching during MCMC without affecting the posterior
659 probability distribution. We obtained genotype estimates as the posterior mean allele count for
660 each individual and locus across chains and values of k (i.e., this integrates over uncertainty in
661 the number of hypothetical source populations). We summarized patterns of population structure
662 and admixture across the sampled populations and individuals based on these admixture
663 proportions for k=2 and a principal component analysis (PCA) of the genotypic data. We then
664 used the prcomp function (Kassambara 2019) to perform a PCA in R (3.4) on the centered, but
665 unstandardized genotype matrix.

666 **ACKNOWLEDGEMENTS**

667 SC was supported by the Utah State University College of Science and School of Graduate
668 Studies. MM was supported by Swiss National Science Foundation Postdoc Mobility grants
669 PBBSP3_141367 and P300P3_147888. ZG was supported by the US NSF (DEB 1844941). This
670 study is part of a project that has received funding from the European Research Council (ERC),
671 to PN, under the European Union’s Horizon 2020 research and innovation programme (Grant
672 agreement No. 770826 EE-Dynamics). The support and resources from the Center for High
673 Performance Computing at the University of Utah are gratefully acknowledged.

674 **AUTHOR CONTRIBUTIONS**

675 PN, MM, OO, ZG, and SC designed the study. PN, MM, RR and VS-C collected data. ZG, OO,
676 and SC analyzed the data. SC wrote the manuscript with feedback from all co-authors.

677 **COMPETING INTERESTS**

678 The authors declare no competing interests.

679 **DATA AND CODE AVAILABILITY**

680 DNA sequence data, genome, experimental data and CHC data used in this study are associated
681 with the previously published studies (Gompert, Comeault, et al. 2014; Riesch et al. 2017). The

682 associated DNA sequence data have been archived on NCBI's SRA (Accession: PRJNA356405
683 ID: 356405). Computer code are available on
684 https://github.com/karwaan/Timema_climate_adaptation_genomics. Correspondence for
685 materials (data, scripts, or samples) should be addressed to Samridhi Chaturvedi
686 (samridhi.chaturvedi@gmail.com) or Zachariah Gompert (zach.gompert@usu.edu) or Patrik
687 Nosil (patrik.nosil@cefe.cnrs.fr).

- 688 **REFERENCES**
- 689 Arendt, Jeff, and David Reznick. 2008. “Convergence and Parallelism Reconsidered: What Have
690 We Learned about the Genetics of Adaptation?” *Trends in Ecology & Evolution* 23 (1):
691 26–32.
- 692 Bailey, Susan F., Nicolas Rodrigue, and Rees Kassen. 2015. “The Effect of Selection
693 Environment on the Probability of Parallel Evolution.” *Molecular Biology and Evolution*
694 32 (6): 1436–48.
- 695 Barghi, Neda, Joachim Hermisson, and Christian Schlötterer. 2020. “Polygenic Adaptation: A
696 Unifying Framework to Understand Positive Selection.” *Nature Reviews. Genetics* 21
697 (12): 769–81.
- 698 Barrett, Rowan D. H., and Dolph Schlüter. 2008. “Adaptation from Standing Genetic Variation.”
699 *Trends in Ecology & Evolution* 23 (1): 38–44.
- 700 Bay, Rachael A., Eric B. Taylor, and Dolph Schlüter. 2019. “Parallel Introgression and Selection
701 on Introduced Alleles in a Native Species.” *Molecular Ecology* 28 (11): 2802–13.
- 702 Blanco-Pastor, José Luis, Isabel M. Liberal, Muhammet Sakiroglu, Yanling Wei, E. Charles
703 Brummer, Rose L. Andrew, and Bernard E. Pfeil. 2021. “Annual and Perennial Medicago
704 Show Signatures of Parallel Adaptation to Climate and Soil in Highly Conserved Genes.”
705 *Molecular Ecology*, no. mec.16061 (July). <https://doi.org/10.1111/mec.16061>.
- 706 Blount, Zachary D., Richard E. Lenski, and Jonathan B. Losos. 2018. “Contingency and
707 Determinism in Evolution: Replaying Life’s Tape.” *Science (New York, N.Y.)* 362 (6415):
708 eaam5979.
- 709 Bohutínská, Magdalena, Jakub Vlček, Sivan Yair, Benjamin Laenen, Veronika Konečná, Marco
710 Fracassetti, Tanja Slotte, and Filip Kolář. 2021. “Genomic Basis of Parallel Adaptation
711 Varies with Divergence in *Arabidopsis* and Its Relatives.” *Proceedings of the National
712 Academy of Sciences of the United States of America* 118 (21): e2022713118.
- 713 Bolnick, Daniel I., Rowan D. H. Barrett, Krista B. Oke, Diana J. Rennison, and Yoel E. Stuart.
714 2018. “(Non)Parallel Evolution.” *Annual Review of Ecology, Evolution, and Systematics*
715 49 (1): 303–30.
- 716 Clarke, Ralph T., Peter Rothery, and Alan F. Raybould. 2002. “Confidence Limits for
717 Regression Relationships between Distance Matrices: Estimating Gene Flow with
718 Distance.” *Journal of Agricultural, Biological, and Environmental Statistics* 7 (3): 361–
719 72.
- 720 Colosimo, Pamela F., Kim E. Hosemann, Sarita Balabhadra, Guadalupe Villarreal Jr, Mark
721 Dickson, Jane Grimwood, Jeremy Schmutz, Richard M. Myers, Dolph Schlüter, and
722 David M. Kingsley. 2005. “Widespread Parallel Evolution in Sticklebacks by Repeated
723 Fixation of Ectodysplasin Alleles.” *Science (New York, N.Y.)* 307 (5717): 1928–33.
- 724 Comeault, Aaron A., Clarissa F. Carvalho, Stuart Dennis, Víctor Soria-Carrasco, and Patrik
725 Nosil. 2016. “Color Phenotypes Are under Similar Genetic Control in Two Distantly
726 Related Species OfTimemastick Insect.” *Evolution; International Journal of Organic
727 Evolution* 70 (6): 1283–96.
- 728 Conte, Gina L., Matthew E. Arnegard, Catherine L. Peichel, and Dolph Schlüter. 2012. “The
729 Probability of Genetic Parallelism and Convergence in Natural Populations.”
730 *Proceedings. Biological Sciences* 279 (1749): 5039–47.
- 731 Danecek, Petr, James K. Bonfield, Jennifer Liddle, John Marshall, Valeriu Ohan, Martin O.
732 Pollard, Andrew Whitwham, et al. 2021. “Twelve Years of SAMtools and BCFtools.”
733 *GigaScience* 10 (2). <https://doi.org/10.1093/gigascience/giab008>.

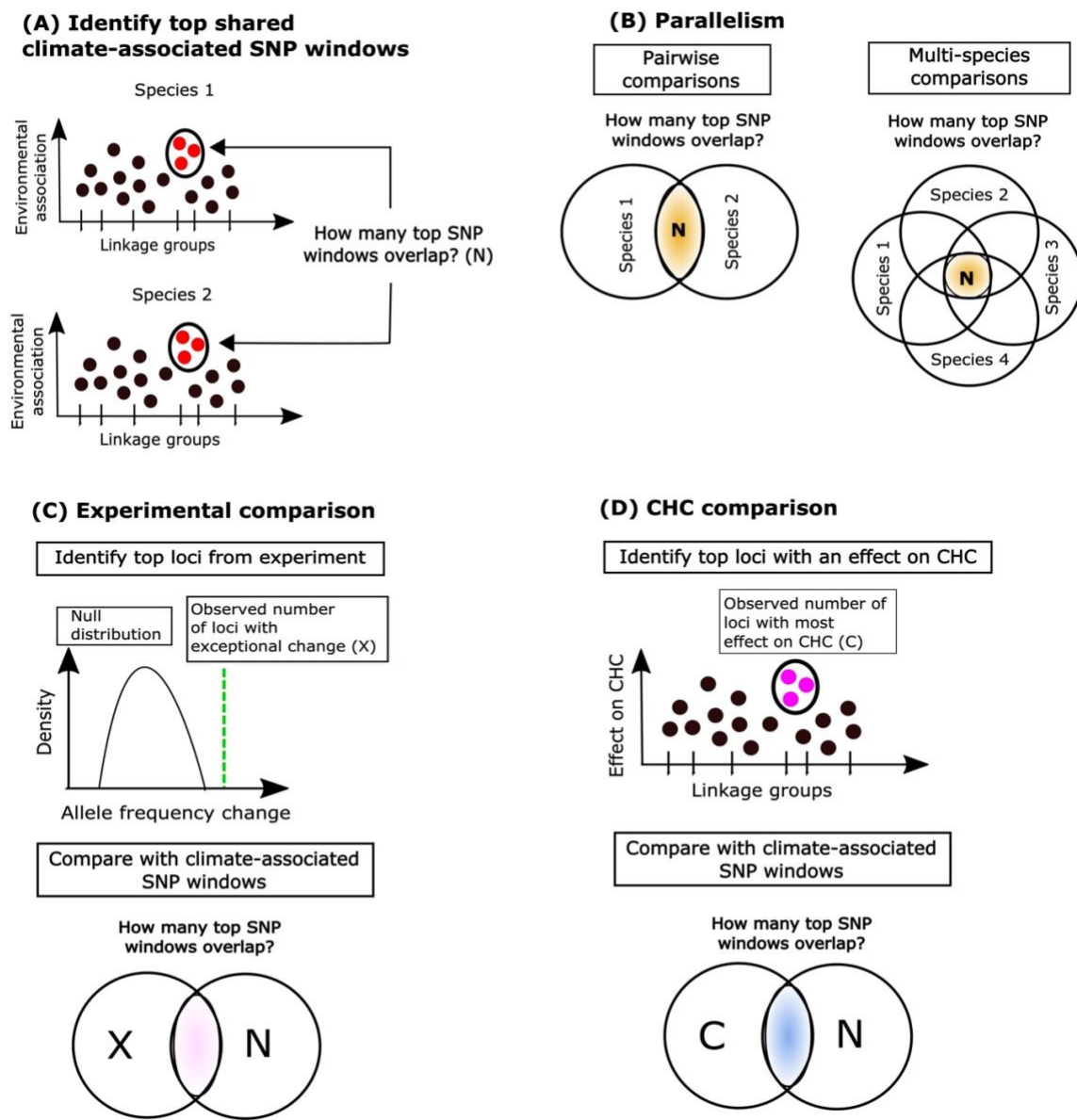
- 734 Elmer, Kathryn R., and Axel Meyer. 2011. "Adaptation in the Age of Ecological Genomics:
735 Insights from Parallelism and Convergence." *Trends in Ecology & Evolution* 26 (6): 298–
736 306.
- 737 Gautier, Mathieu. 2015. "Genome-Wide Scan for Adaptive Divergence and Association with
738 Population-Specific Covariates." *Genetics* 201 (4): 1555–79.
- 739 Giska, Iwona, Liliana Farelo, João Pimenta, Fernando A. Seixas, Mafalda S. Ferreira, João P.
740 Marques, Inês Miranda, et al. 2019. "Introgression Drives Repeated Evolution of Winter
741 Coat Color Polymorphism in Hares." *Proceedings of the National Academy of Sciences
742 of the United States of America* 116 (48): 24150–56.
- 743 Gompel, Nicolas, and Sean B. Carroll. 2003. "Genetic Mechanisms and Constraints Governing
744 the Evolution of Correlated Traits in Drosophilid Flies." *Nature* 424 (6951): 931–35.
- 745 Gompert, Zachariah, Aaron A. Comeault, Timothy E. Farkas, Jeffrey L. Feder, Thomas L.
746 Parchman, C. Alex Buerkle, and Patrik Nosil. 2014. "Experimental Evidence for
747 Ecological Selection on Genome Variation in the Wild." *Ecology Letters* 17 (3): 369–79.
- 748 Gompert, Zachariah, Lauren K. Lucas, C. Alex Buerkle, Matthew L. Forister, James A. Fordyce,
749 and Chris C. Nice. 2014. "Admixture and the Organization of Genetic Diversity in a
750 Butterfly Species Complex Revealed through Common and Rare Genetic Variants."
751 *Molecular Ecology* 23 (18): 4555–73.
- 752 Good, Benjamin H., Michael J. McDonald, Jeffrey E. Barrick, Richard E. Lenski, and Michael
753 M. Desai. 2017. "The Dynamics of Molecular Evolution over 60,000 Generations."
754 *Nature* 551 (7678): 45–50.
- 755 Gould, Stephen Jay. 1990. *Wonderful Life*. London, England: Radius.
- 756 Grant, Peter R., and B. Rosemary Grant. 2002. "Unpredictable Evolution in a 30-Year Study of
757 Darwin's Finches." *Science (New York, N.Y.)* 296 (5568): 707–11.
- 758 Greenway, Ryan, Nick Barts, Chathurika Henpita, Anthony P. Brown, Lenin Arias Rodriguez,
759 Carlos M. Rodríguez Peña, Sabine Arndt, et al. 2020. "Convergent Evolution of
760 Conserved Mitochondrial Pathways Underlies Repeated Adaptation to Extreme
761 Environments." *Proceedings of the National Academy of Sciences of the United States of
762 America* 117 (28): 16424–30.
- 763 Günther, Torsten, and Graham Coop. 2013. "Robust Identification of Local Adaptation from
764 Allele Frequencies." *Genetics* 195 (1): 205–20.
- 765 Haldane, John Burdon. 1990. *The Causes of Evolution*. Princeton Science Library 5. Princeton,
766 NJ: Princeton University Press.
- 767 Heliconius Genome Consortium. 2012. "Butterfly Genome Reveals Promiscuous Exchange of
768 Mimicry Adaptations among Species." *Nature* 487 (7405): 94–98.
- 769 Henning, Frederico, and Axel Meyer. 2014. "The Evolutionary Genomics of Cichlid Fishes:
770 Explosive Speciation and Adaptation in the Postgenomic Era." *Annual Review of
771 Genomics and Human Genetics* 15 (1): 417–41.
- 772 Kassambara, Alboukadel. 2019. *Practical Statistics in R for Comparing Groups*. Practical
773 Statistics in R 2. Independently Published.
- 774 Kingsley, Evan P., Marie Manceau, Christopher D. Wiley, and Hopi E. Hoekstra. 2009.
775 "Melanism in Peromyscus Is Caused by Independent Mutations in Agouti." *PloS One* 4
776 (7): e6435.
- 777 Kohler, Annegret, Alan Kuo, Laszlo G. Nagy, Emmanuelle Morin, Kerrie W. Barry, Francois
778 Buscot, Björn Canbäck, et al. 2015. "Convergent Losses of Decay Mechanisms and

- 779 Rapid Turnover of Symbiosis Genes in Mycorrhizal Mutualists.” *Nature Genetics* 47 (4):
780 410–15.
- 781 Langerhans, R. Brian. 2010. “Predicting Evolution with Generalized Models of Divergent
782 Selection: A Case Study with Poeciliid Fish.” *Integrative and Comparative Biology* 50
783 (6): 1167–84.
- 784 Law, Jennifer H., and Bernard J. Crespi. 2002. “The Evolution of Geographic Parthenogenesis in
785 Timema Walking-Sticks.” *Molecular Ecology* 11 (8): 1471–89.
- 786 Lenski, Richard E. 2017. “Experimental Evolution and the Dynamics of Adaptation and Genome
787 Evolution in Microbial Populations.” *The ISME Journal* 11 (10): 2181–94.
- 788 Li, Heng. 2013. “Aligning Sequence Reads, Clone Sequences and Assembly Contigs with BWA-
789 MEM.” *ArXiv [q-Bio.GN]*. arXiv. <http://arxiv.org/abs/1303.3997>.
- 790 Li, Heng, Bob Handsaker, Alec Wysoker, Tim Fennell, Jue Ruan, Nils Homer, Gabor Marth,
791 Goncalo Abecasis, Richard Durbin, and 1000 Genome Project Data Processing
792 Subgroup. 2009. “The Sequence Alignment/Map Format and SAMtools.” *Bioinformatics*
793 (Oxford, England) 25 (16): 2078–79.
- 794 Lieberman, Tami D., Jean-Baptiste Michel, Mythili Aingaran, Gail Potter-Bynoe, Damien Roux,
795 Michael R. Davis Jr, David Skurnik, et al. 2011. “Parallel Bacterial Evolution within
796 Multiple Patients Identifies Candidate Pathogenicity Genes.” *Nature Genetics* 43 (12):
797 1275–80.
- 798 Lindtke, Dorothea, Kay Lucek, Víctor Soria-Carrasco, Romain Villoutreix, Timothy E. Farkas,
799 Rüdiger Riesch, Stuart R. Dennis, Zach Gompert, and Patrik Nosil. 2017. “Long-Term
800 Balancing Selection on Chromosomal Variants Associated with Cryspsis in a Stick
801 Insect.” *Molecular Ecology* 26 (22): 6189–6205.
- 802 Linnen, Catherine R., Yu-Ping Poh, Brant K. Peterson, Rowan D. H. Barrett, Joanna G. Larson,
803 Jeffrey D. Jensen, and Hopi E. Hoekstra. 2013. “Adaptive Evolution of Multiple Traits
804 through Multiple Mutations at a Single Gene.” *Science (New York, N.Y.)* 339 (6125):
805 1312–16.
- 806 Losos, Jonathan B. 2011. “Convergence, Adaptation, and Constraint.” *Evolution; International
807 Journal of Organic Evolution* 65 (7): 1827–40.
- 808 Manceau, Marie, Vera S. Domingues, Catherine R. Linnen, Erica Bree Rosenblum, and Hopi E.
809 Hoekstra. 2010. “Convergence in Pigmentation at Multiple Levels: Mutations, Genes and
810 Function.” *Philosophical Transactions of the Royal Society of London. Series B,
811 Biological Sciences* 365 (1552): 2439–50.
- 812 Manousaki, Tereza, Pincelli M. Hull, Henrik Kusche, Gonzalo Machado-Schiaffino, Paolo
813 Franchini, Chris Harrod, Kathryn R. Elmer, and Axel Meyer. 2013. “Parsing Parallel
814 Evolution: Ecological Divergence and Differential Gene Expression in the Adaptive
815 Radiations of Thick-Lipped Midas Cichlid Fishes from Nicaragua.” *Molecular Ecology*
816 22 (3): 650–69.
- 817 Marburger, Sarah, Patrick Monnahan, Paul J. Seear, Simon H. Martin, Jordan Koch, Pirita
818 Paaajanen, Magdalena Bohutínská, James D. Higgins, Roswitha Schmickl, and Levi Yant.
819 2019. “Interspecific Introgression Mediates Adaptation to Whole Genome Duplication.”
820 *Nature Communications* 10 (1): 5218.
- 821 Matos, Margarida, Pedro Simões, Marta A. Santos, Sofia G. Seabra, Gonçalo S. Faria, Filipa
822 Vala, Josiane Santos, and Inês Fragata. 2015. “History, Chance and Selection during
823 Phenotypic and Genomic Experimental Evolution: Replaying the Tape of Life at
824 Different Levels.” *Frontiers in Genetics* 6 (February): 71.

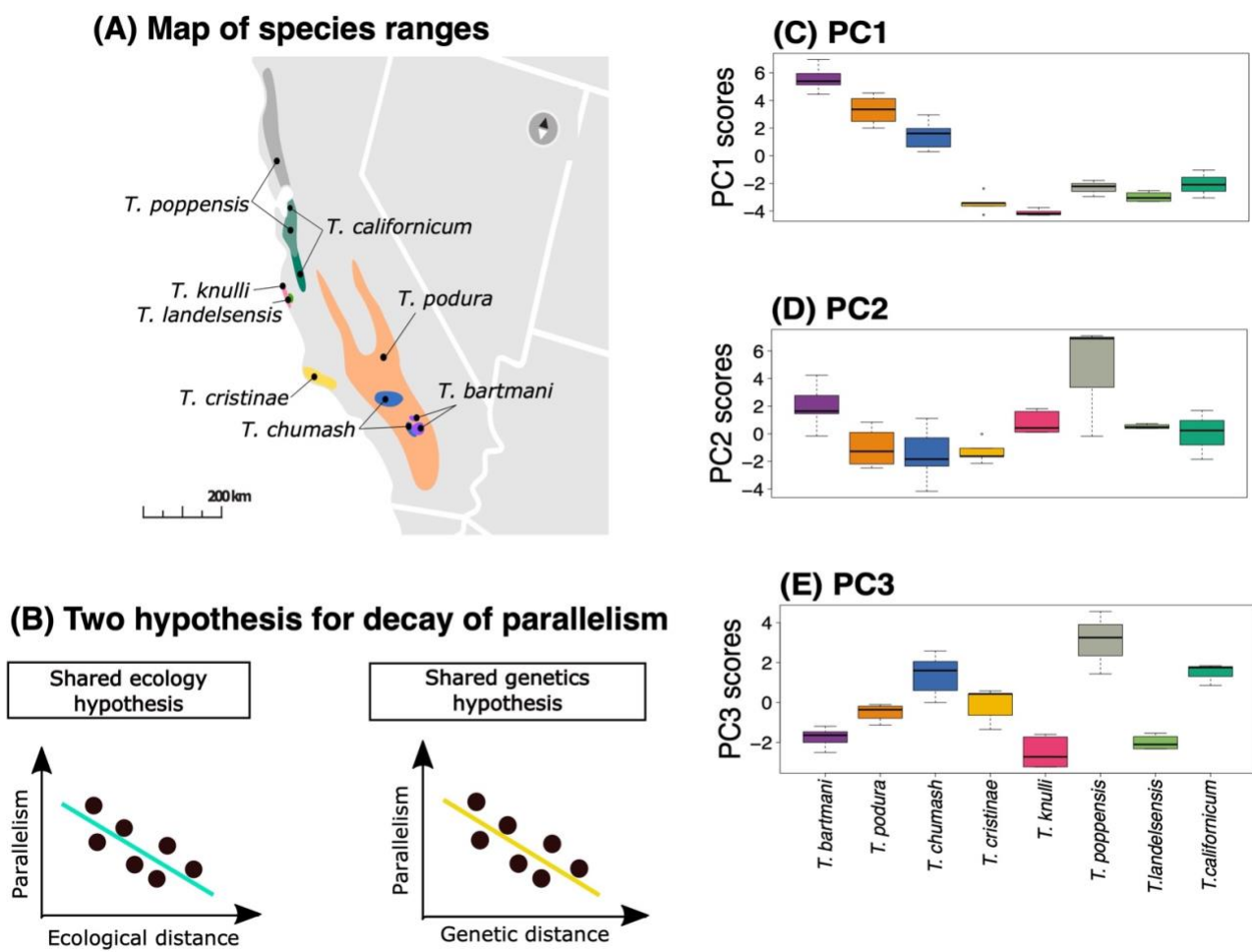
- 825 Menon, Mitra, Justin C. Bagley, Gerald F. M. Page, Amy V. Whipple, Anna W. Schoettle,
826 Christopher J. Still, Christian Wehenkel, et al. 2021. “Adaptive Evolution in a Conifer
827 Hybrid Zone Is Driven by a Mosaic of Recently Introgressed and Background Genetic
828 Variants.” *Communications Biology* 4 (1): 160.
- 829 Morales, Hernán E., Rui Faria, Kerstin Johannesson, Tomas Larsson, Marina Panova, Anja M.
830 Westram, and Roger K. Butlin. 2019. “Genomic Architecture of Parallel Ecological
831 Divergence: Beyond a Single Environmental Contrast.” *Science Advances* 5 (12):
832 eaav9963.
- 833 Nosil, Patrik. 2007. “Divergent Host Plant Adaptation and Reproductive Isolation between
834 Ecotypes of *Timema cristinae* Walking Sticks.” *The American Naturalist* 169 (2): 151–
835 62.
- 836 Nosil, Patrik, Romain Villoutreix, Clarissa F. de Carvalho, Timothy E. Farkas, Víctor Soria-
837 Carrasco, Jeffrey L. Feder, Bernard J. Crespi, and Zach Gompert. 2018. “Natural
838 Selection and the Predictability of Evolution in *Timema* Stick Insects.” *Science*,
839 February. <https://science.science.org/content/359/6377/765>.
- 840 Nosil, Patrik, Romain Villoutreix, Clarissa F. de Carvalho, Jeffrey L. Feder, Thomas L.
841 Parchman, and Zach Gompert. 2020. “Ecology Shapes Epistasis in a Genotype-
842 Phenotype-Fitness Map for Stick Insect Colour.” *Nature Ecology & Evolution* 4 (12):
843 1673–84.
- 844 Orgogozo, Virginie. 2015. “Replaying the Tape of Life in the Twenty-First Century.” *Interface
845 Focus* 5 (6): 20150057.
- 846 Papadopoulos, Alexander S. T., Andrew J. Helmstetter, Owen G. Osborne, Aaron A. Comeault,
847 Daniel P. Wood, Edward A. Straw, Laurence Mason, et al. 2021. “Rapid Parallel
848 Adaptation to Anthropogenic Heavy Metal Pollution.” *Molecular Biology and Evolution*
849 38 (9): 3724–36.
- 850 Pickrell, Joseph K., and Jonathan K. Pritchard. 2012. “Inference of Population Splits and
851 Mixtures from Genome-Wide Allele Frequency Data.” *PLoS Genetics* 8 (11): e1002967.
- 852 Pritchard, J. K., M. Stephens, and P. Donnelly. 2000. “Inference of Population Structure Using
853 Multilocus Genotype Data.” *Genetics* 155 (2): 945–59.
- 854 Rajpurohit, S., R. Hanus, V. Vrkoslav, E. L. Behrman, A. O. Bergland, D. Petrov, J. Cvačka, and
855 P. S. Schmidt. 2017. “Adaptive Dynamics of Cuticular Hydrocarbons in *Drosophila*.”
856 *Journal of Evolutionary Biology* 30 (1): 66–80.
- 857 Rennison, Diana J., Kira E. Delmore, Kieran Samuk, Gregory L. Owens, and Sara E. Miller.
858 2020. “Shared Patterns of Genome-Wide Differentiation Are More Strongly Predicted by
859 Geography than by Ecology.” *The American Naturalist* 195 (2): 192–200.
- 860 Riesch, Rüdiger, Moritz Muschick, Dorothea Lindtke, Romain Villoutreix, Aaron A. Comeault,
861 Timothy E. Farkas, Kay Lucek, et al. 2017. “Transitions between Phases of Genomic
862 Differentiation during Stick-Insect Speciation.” *Nature Ecology & Evolution* 1 (4): 82.
- 863 Rockman, Matthew V. 2012. “The QTN Program and the Alleles That Matter for Evolution: All
864 That’s Gold Does Not Glitter.” *Evolution; International Journal of Organic Evolution* 66
865 (1): 1–17.
- 866 Roda, Federico, Huanle Liu, Melanie J. Wilkinson, Gregory M. Walter, Maddie E. James, Diana
867 M. Bernal, Maria C. Melo, et al. 2013. “Convergence and Divergence during the
868 Adaptation to Similar Environments by an Australian Groundsel.” *Evolution;
869 International Journal of Organic Evolution* 67 (9): 2515–29.

- 870 Roesti, Marius, Sergey Gavrillets, Andrew P. Hendry, Walter Salzburger, and Daniel Berner.
871 2014. "The Genomic Signature of Parallel Adaptation from Shared Genetic Variation."
872 *Molecular Ecology* 23 (16): 3944–56.
- 873 Rose, Noah H., Rachael A. Bay, Megan K. Morikawa, and Stephen R. Palumbi. 2018.
874 "Polygenic Evolution Drives Species Divergence and Climate Adaptation in Corals."
875 *Evolution; International Journal of Organic Evolution* 72 (1): 82–94.
- 876 Schluter, Dolph, Elizabeth A. Clifford, Maria Nemethy, and Jeffrey S. McKinnon. 2004.
877 "Parallel Evolution and Inheritance of Quantitative Traits." *The American Naturalist* 163
878 (6): 809–22.
- 879 Soria-Carrasco, Víctor, Zachariah Gompert, Aaron A. Comeault, Timothy E. Farkas, Thomas L.
880 Parchman, J. Spencer Johnston, C. Alex Buerkle, et al. 2014. "Stick Insect Genomes
881 Reveal Natural Selection's Role in Parallel Speciation." *Science (New York, N.Y.)* 344
882 (6185): 738–42.
- 883 Stern, David L. 2013. "The Genetic Causes of Convergent Evolution." *Nature Reviews. Genetics*
884 14 (11): 751–64.
- 885 Stern, David L., and Virginie Orgogozo. 2009. "Is Genetic Evolution Predictable?" *Science (New*
886 *York, N.Y.)* 323 (5915): 746–51.
- 887 Storz, Jay F. 2016. "Causes of Molecular Convergence and Parallelism in Protein Evolution."
888 *Nature Reviews. Genetics* 17 (4): 239–50.
- 889 Stuart, Yoel E., Thor Veen, Jesse N. Weber, Dieta Hanson, Mark Ravinet, Brian K. Lohman,
890 Cole J. Thompson, et al. 2017. "Contrasting Effects of Environment and Genetics
891 Generate a Continuum of Parallel Evolution." *Nature Ecology & Evolution* 1 (6): 158.
- 892 Villoutreix, Romain, Clarissa F. de Carvalho, Víctor Soria-Carrasco, Dorothea Lindtke, Marisol
893 De-la-Mora, Moritz Muschick, Jeffrey L. Feder, Thomas L. Parchman, Zach Gompert,
894 and Patrik Nosil. 2020. "Large-Scale Mutation in the Evolution of a Gene Complex for
895 Cryptic Coloration." *Science (New York, N.Y.)* 369 (6502): 460–66.
- 896 Walden, Nora, Kay Lucek, and Yvonne Willi. 2020. "Lineage-Specific Adaptation to Climate
897 Involves Flowering Time in North American *Arabidopsis Lyrata*." *Molecular Ecology* 29
898 (8): 1436–51.
- 899 Waldvogel, Ann-Marie, Barbara Feldmeyer, Gregor Rolshausen, Moises Exposito-Alonso,
900 Christian Rellstab, Robert Kofler, Thomas Mock, et al. 2020. "Evolutionary Genomics
901 Can Improve Prediction of Species' Responses to Climate Change." *Evolution Letters* 4
902 (1): 4–18.
- 903 Yeaman, Sam. 2015. "Local Adaptation by Alleles of Small Effect." *The American Naturalist*
904 186 Suppl 1 (S1): S74–89.
- 905 Yeaman, Sam, Kathryn A. Hodgins, Katie E. Lotterhos, Haktan Suren, Simon Nadeau, Jon C.
906 Degner, Kristin A. Nurkowski, et al. 2016. "Convergent Local Adaptation to Climate in
907 Distantly Related Conifers." *Science (New York, N.Y.)* 353 (6306): 1431–33.
- 908 Zhang, Xiao, Jack G. Rayner, Mark Blaxter, and Nathan W. Bailey. 2021. "Rapid Parallel
909 Adaptation despite Gene Flow in Silent Crickets." *Nature Communications* 12 (1): 50.
- 910 Zhou, Xiang, Peter Carbonetto, and Matthew Stephens. 2013. "Polygenic Modeling with
911 Bayesian Sparse Linear Mixed Models." *PLoS Genetics* 9 (2): e1003264.

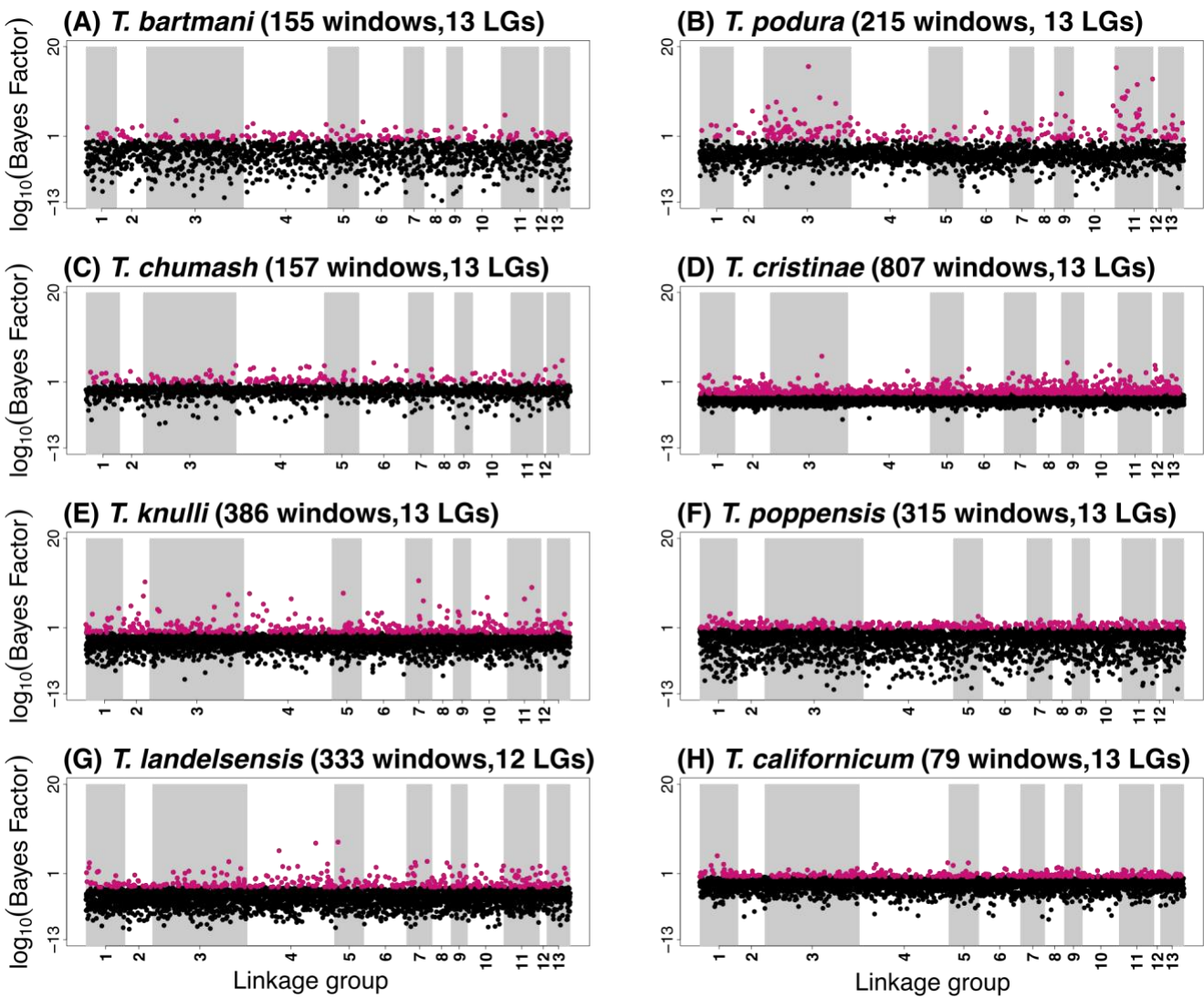
913 Figure 1: Conceptual figure to summarize the analyses conducted in this study. (A) Diagram shows the approach to
 914 quantify overlap of top climate-associated SNP windows between a given pair of species (Species 1 and species 2).
 915 Here red dots denote climate-associated SNP windows for each species. We then quantify overlap in these windows
 916 between the two species (“N”). (B) Parallelism: Diagram shows the approach to quantify excess overlap of top
 917 climate-associated SNP windows between a given pair of species (“pairwise comparison”) and for multiple species
 918 (“multi-species comparison”). (C) Experimental comparison: Diagram shows two steps to identify excess overlap in
 919 climate-associated SNP windows and that changed in an elevation-dependent manner during an experiment. Here,
 920 first we identify loci/genomic regions associated with the greatest allele frequency change in an elevational
 921 dependent manner in an experiment as those which show exceptional change as compared to a null expectation
 922 (denoted in green line, denoted as “X”). Second, we compare if these regions (“X”) show excess overlap with the
 923 climate associated SNP windows (“N”). (D) CHC comparison: Diagram shows two steps to identify excess overlap
 924 in climate-associated SNP windows and genomic regions associated with CHCs. First we identify loci/genomic
 925 regions associated with greatest effect on CHC traits (denoted in green line, denoted as “C”). Second, we compare if
 926 these regions (“C”) show excess overlap with the climate associated SNP windows (“N”).



928 Figure 2: Map of species range and plots for within species variation in climate PC scores. (A)
 929 Map of the ranges of the eight species included in the study, where the coloured shapes represent
 930 the geographic ranges of each species. (B) Two hypotheses which we use to test for decay of
 931 parallelism: First diagram shows our prediction for the “shared ecology” hypothesis where we
 932 expect a decay in parallelism with an increase in ecological (i.e., climate) distance. Second
 933 diagram shows our prediction for the “shared genetics” hypothesis where we expect a decay in
 934 parallelism with an increase in genetic distance. We use these two hypotheses to study the decay
 935 of parallelism. (C-E) Box plots of PC variation for the first three principal components (PC1,
 936 PC2, PC3) for the eight species included in the study ($n = 1420$ individuals from 53 localities).



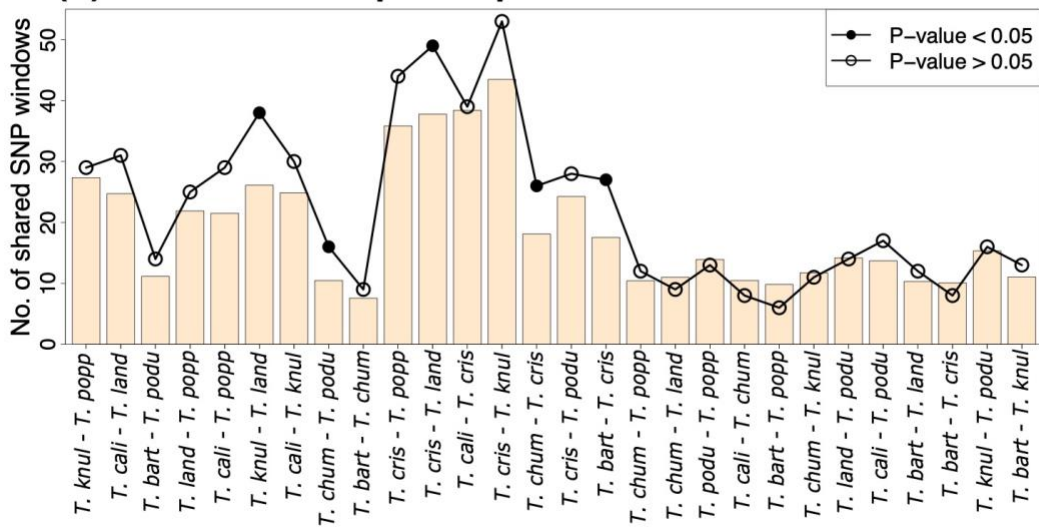
938 Figure 3: Manhattan plots showing the strength of evidence for association (measured here using
 939 the Bayes factor from the software BayPass) between a SNP window and climate (in this case,
 940 PC3, see Figures S2 and S3 for analogous results for PC1 and PC2). Results are shown along the
 941 13 linkage groups. Red points denote the SNP windows in the top 10% quantile (i.e., referred to
 942 as 'climate-associated SNP windows' throughout the main text). In each panel title, the two
 943 values in parentheses are the number of SNP windows in the top 10% quantile ("windows"),
 944 followed by the number of linkage groups with at least 1 SNP window in the top 10% quantile
 945 ("LGs").



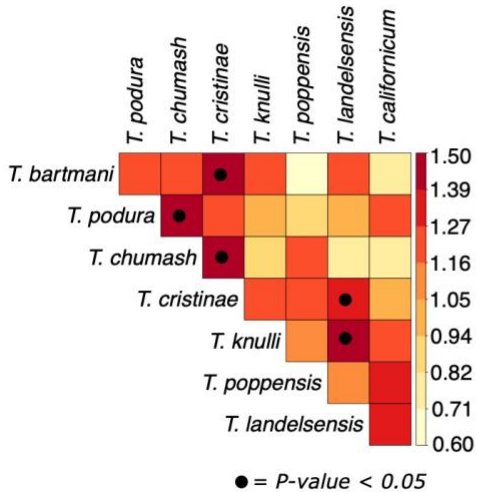
946

947 Figure 4: Tests for parallel climate-associated SNP windows between and among species of
 948 *Timema* stick insects (all plots are for the top 10% empirical quantile). In this case, PC3, see
 949 Figures S4 and S5 for analogous results for PC1 and PC2. (A) Plot shows observed versus
 950 expected number of overlapping climate-associated SNP windows for species pairwise
 951 comparison for PC3. Bars denote expected values and solid lines denotes observed values. Open
 952 points indicate P-value > 0.05 and filled points indicate P-value ≤ 0.05. (B) Pairwise plot shows
 953 x-fold enrichment values for each comparison between pairs of species. Black dot on each box
 954 denotes P-value ≤ 0.05. (C) Plot shows x-fold enrichments for number of overlapping climate-
 955 associated SNP windows for PC3 for comparisons between multiple species, i.e., beyond pairs of
 956 species (e.g., 2 or more species, 3 or more species, 4 or more species). Bars denote observed x-
 957 fold value for each multi-species comparison. Black lines on bars show the 95% confidence
 958 intervals. N value above each bar indicates the observed number of overlapping climate-
 959 associated SNP windows for each comparison. * Indicates x-fold enrichments with P-value ≤
 960 0.05.

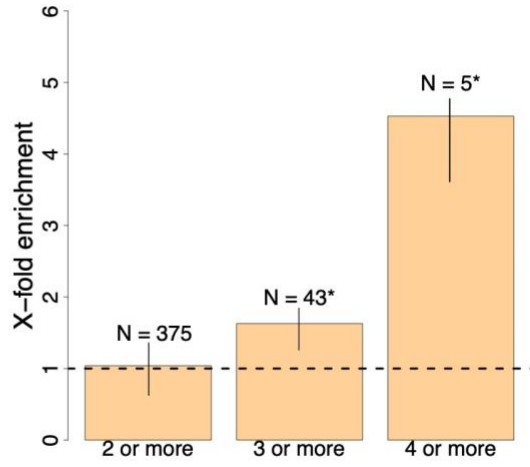
(A) Observed vs. expected parallelism



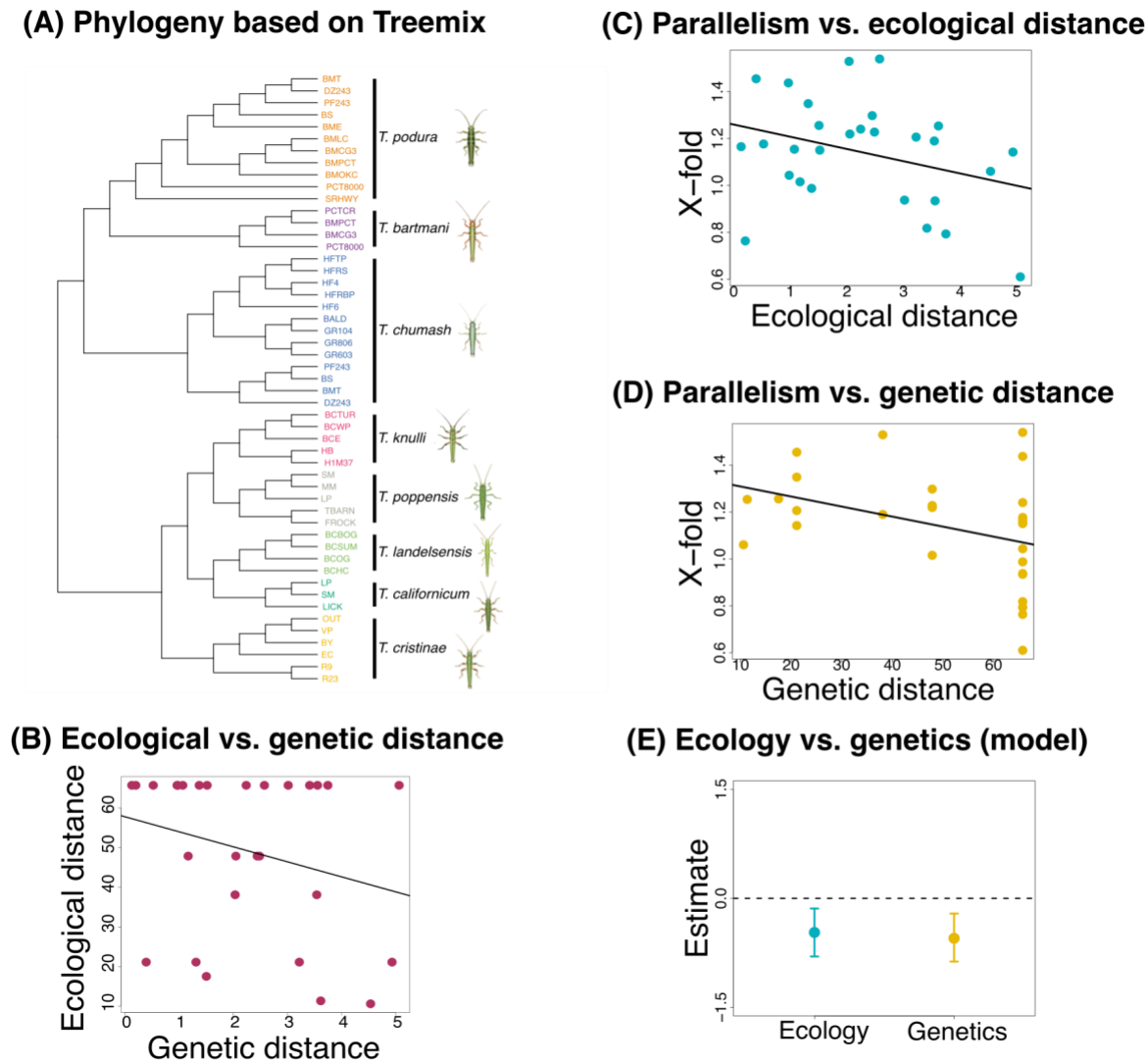
(B) Pairwise comparisons



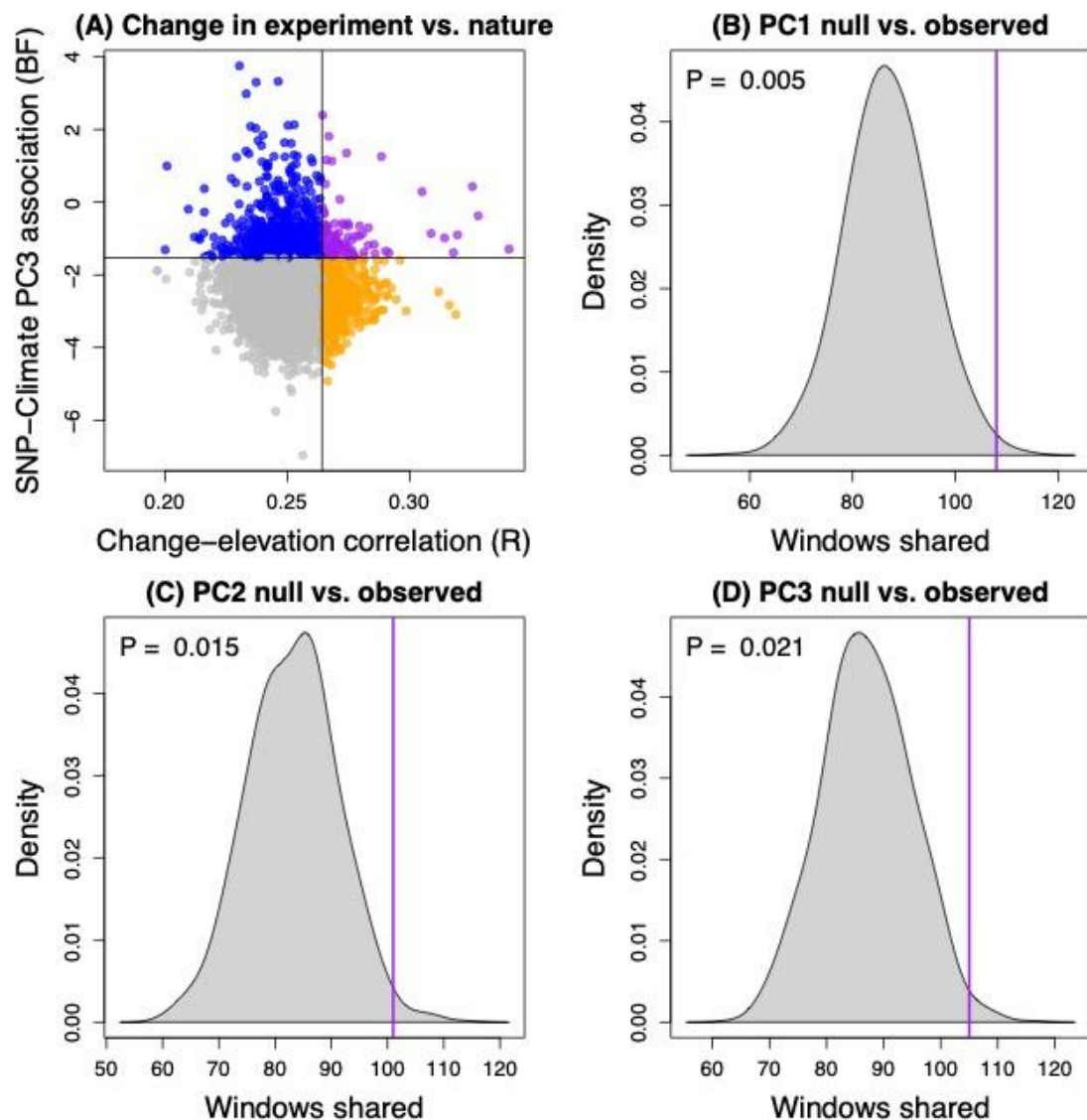
(C) Multi-species comparisons



962 Figure 5: Tests for introgression and “shared ecology” and “shared genetics” hypotheses. (A)
 963 Population graph from TREEMIX for all *Timema* populations used in this study ($N = 53$),
 964 allowing no migration or admixture event (the actual migration edge is not shown due to the
 965 proportion of variation explained from the admixture model as shown in Table S9). Terminal
 966 nodes are labelled by abbreviations for locations from where samples were collected and
 967 coloured according to species. (B) Scatterplot shows the relationship between ecological distance
 968 (measured as distance in PC3 scores and is distance in climate variables) and genetic distance
 969 (measured as pairwise phylogenetic distance). (C) Scatterplot shows the relationship between x-
 970 fold enrichment (measure for parallelism) and ecological distance (measured as distance in PC3
 971 scores) (D) Scatterplot shows the relationship between X-fold enrichment (measure for
 972 parallelism) and genetic distance (measured as pairwise phylogenetic distance). (E) Plot shows
 973 parameter estimates with standardized coefficients for the full model for PC3. Estimates
 974 diverging from zero indicate a positive or negative effect of ecology or genetics on parallelism.
 975 Analogous results for (B)- (E) are shown in figure S8 and S9 for PC1 and PC2. A negative or
 976 positive estimate which deviates from zero is indicative of effect on parallelism.



978 Figure 6. Evidence for excess overlap between 100kb windows associated with climate in nature
 979 and that changed in an elevation-dependent manner during an experiment. (A) The scatterplot
 980 shows the mean correlation between change and elevation during an experiment versus the
 981 median Bayes factor measuring SNP-climate (PC3) association in nature for *T. cristinae* for 100
 982 kb windows. Points denoting windows in the top 10% for change-elevation correlations are
 983 shown in orange, those in the top 10% for SNP-climate associations are shown in blue, and those
 984 in the top 10% for both are in purple (other windows are shown with gray points). We are
 985 interested in the top right corner of the plot, that is the purple points denoting windows were
 986 exceptional (top 10%) in the experiment and nature, and we used a randomization test to ask
 987 whether more windows fall in this category than expected by chance. Panels (B), (C) and (D)
 988 show null expectations for the number of windows in the top 10% for the experiment and nature
 989 based on climate PCs 1, 2 and 3, respectively. The null distribution from the constrained
 990 randomization test in each case is denoted by the gray density plot, whereas the observed value is
 991 shown with a vertical purple line. The *P*-value for the null hypothesis of no association between
 992 SNP-climate and change-elevation correlations is reported in each panel as well.



993

994 **SUPPLEMENTARY TABLES AND FIGURES**

995 Table S1: Locality information and sample sizes for the eight species and 53 localities for which
 996 the GBS data has been included in this study. The GBS data associated with these populations
 997 and individuals was first presented in Riesch et al. 2017.

Species	No. of populations	No. of individuals
<i>T. bartmani</i>	6	195
<i>T. californicum</i>	3	77
<i>T. chumash</i>	12	358
<i>T. cristinae</i>	6	205
<i>T. knulli</i>	5	89
<i>T. landelsensis</i>	4	125
<i>T. podura</i>	12	255
<i>T. poppensis</i>	5	116

998

999
1000 Table S2: Details of climate variables included in this study and their principal component scores
1001 for first three PCs (Total proportion of variation explained by each PC: PC1 = 51.7%, PC2 =
24.4% and PC3 = 16.1%).

Code	Description	PC1	PC2	PC3
BIO1	Annual Mean Temperature	-0.24	0.21	0.15
BIO2	Mean Diurnal Range (Mean of monthly (max temp - min temp))	0.17	0.19	0.03
BIO3	Isothermality (BIO2/BIO7) ($\times 100$)	-0.22	-0.12	-0.24
BIO4	Temperature Seasonality (standard deviation $\times 100$)	0.25	0.16	0.19
BIO5	Max Temperature of Warmest Month	0.06	0.33	0.31
BIO6	Min Temperature of Coldest Month	-0.29	0.03	0.04
BIO7	Temperature Annual Range (BIO5-BIO6)	0.25	0.19	0.17
BIO8	Mean Temperature of Wettest Quarter	-0.29	0.08	0.03
BIO9	Mean Temperature of Driest Quarter	-0.1	0.29	0.34
BIO10	Mean Temperature of Warmest Quarter	-0.02	0.34	0.33
BIO11	Mean Temperature of Coldest Quarter	-0.29	0.06	0.01
BIO12	Annual Precipitation	0.09	-0.32	0.31
BIO13	Precipitation of Wettest Month	0.02	-0.32	0.36
BIO14	Precipitation of Driest Month	0.26	-0.14	-0.04
BIO15	Precipitation Seasonality (Coefficient of Variation)	-0.25	-0.01	0.18
BIO16	Precipitation of Wettest Quarter	0.04	-0.31	0.36
BIO17	Precipitation of Driest Quarter	0.27	-0.06	-0.11
BIO18	Precipitation of Warmest Quarter	0.28	-0.05	-0.07
BIO19	Precipitation of Coldest Quarter	0.04	-0.32	0.34
Elev	Elevation	0.29	0	-0.02
Lat	Latitude	-0.19	-0.25	0.08
Long	Longitude	0.25	0.19	-0.02

1002 Table S3. Summary of model posterior predictive performance as approximated by the deviance
 1003 information criterion (DIC) for models predicting parallelism as a function of genes and ecology.
 1004 The full model in each case (for each PC) includes genes and ecology, and the null model
 1005 includes only an intercept term. D gives the mean deviance and pD denotes the effective number
 1006 of parameters. Lower DIC values denote better models.

PC	Model	D	pD	DIC
PC1	Full	51.03	12.17	63.2
	Genes	52.04	11.03	63.1
	Ecology	69.55	10.27	79.8
	Null	76.1	5	81.1
PC2	Full	81.38	4.95	86.3
	Genes	80.59	3.89	84.5
	Ecology	84.18	3.98	85.2
	Null	80.48	2.85	83.3
PC3	Full	68.32	5.64	74
	Genes	74.95	4.51	79.5
	Ecology	78.03	3.88	81.9
	Null	80.2	2.9	83.1

1007

1008 Table S4. Excess overlap between top climate-associations windows and those where change
 1009 was mostly strongly correlated with elevation in the release-recapture experiment. Results are
 1010 shown for different top quantiles. Here 0.90 indicates the top 10% of windows, which
 1011 corresponds to the results in the main text. We report the observed number of windows in the top
 1012 quantiles for both change and climate association, the x-fold enrichment relative to null
 1013 expectations, and the corresponding P-value for each PC climate variable. Results are shown for
 1014 null distributions where all windows were permuted or randomized (“Full randomization”) and
 1015 where randomizations were limited to windows with similar numbers of SNPs (“Constrained
 1016 randomization”). *P*-values $\leq .05$ are highlighted in bold.

PC1					
		Full randomization		Constrained randomization	
Quantile	Observed	X-fold	P-value	X-fold	P-value
0.9	108	1.40	< 0.001	1.24	0.005
0.91	86	1.39	< 0.001	1.19	0.040
0.92	75	1.53	< 0.001	1.29	0.014
0.93	59	1.56	< 0.001	1.29	0.013
0.94	48	1.72	< 0.001	1.36	0.014
0.95	43	2.21	< 0.001	1.65	< 0.001
0.96	33	2.68	< 0.001	1.84	0.001
0.97	25	3.58	< 0.001	2.29	< 0.001
0.98	15	4.83	< 0.001	2.63	0.001
0.99	6	7.47	< 0.001	3.07	0.14
PC2					
		Full randomization		Constrained randomization	
Quantile	Observed	X-fold	P-value	X-fold	P-value
0.9	101	1.32	0.003	1.21	0.015
0.91	77	1.24	0.034	1.12	0.138
0.92	67	1.37	0.005	1.21	0.062
0.93	53	1.39	0.010	1.22	0.064
0.94	44	1.59	0.001	1.32	0.039
0.95	36	1.86	< 0.001	1.45	0.014
0.96	28	2.29	< 0.001	1.66	0.003

0.97	17	2.48	0.001	1.64	0.035
0.98	9	2.92	0.004	1.57	0.122
0.99	2	2.58	0.180	1.15	0.534
PC3					
		Full randomization		Constrained randomization	
Quantile	Observed	X-fold	P-value	X-fold	P-value
0.9	105	1.37	< 0.001	1.21	0.021
0.91	91	1.46	< 0.001	1.27	0.005
0.92	73	1.48	0.001	1.27	0.012
0.93	50	1.32	0.019	1.11	0.232
0.94	40	1.45	0.008	1.17	0.157
0.95	26	1.33	0.068	1.04	0.438
0.96	20	1.60	0.027	1.22	0.188
0.97	12	1.72	0.049	1.25	0.264
0.98	5	1.68	0.188	1.04	0.516
0.99	3	3.95	0.028	2.50	0.103

1017

1018 Table S5. Bayesian estimates of the percent of CHC variation explained by sequenced SNPs.
1019 Estimates are from the polygenic GWA in gemma. The posterior median gives the point estimate
1020 of the percent of CHC variation explained by the SNPs; the 95% equal-tail probability intervals
1021 (ETPIs) are also given.

Trait	Posterior median	95% ETPI
Female pentacosanes	89.7	35.8-99.9
Female heptacosanes	52.5	4.9-98.9
Female nonacosanes	80.2	15.5-99.8
Male pentacosanes	53.2	8.3-97.2
Male heptacosanes	52.4	10.3-96.5
Male nonacosanes	50.8	7.8-95.6

1022

1023 Table S6: X-fold enrichments and associated *P*-values for number of overlapping SNP windows
 1024 for PC1 for comparison with CHC experiment. Observed value gives the mean posterior
 1025 inclusions probability (i.e., probability of a genotype-phenotype association) across all SNPs in
 1026 100 kb windows for each of the six CHC traits. *P*-values $\leq .05$ are highlighted in bold.

<i>T. bartmani</i>				<i>T. podura</i>			
CHC	X-fold	Observed	P-value	CHC	X-fold	Observed	P-value
F-penta	1.06	0.000439	0.128	F-penta	1.07	0.0004425	0.059
F-hepta	1.02	0.000301	0.271	F-hepta	1.01	0.0002928	0.457
F-nona	0.99	0.000264	0.526	F-nona	0.94	0.00024994	0.909
M-penta	0.96	0.000345	0.781	M-penta	0.99	0.00035676	0.551
M-hepta	1.07	0.000508	0.072	M-hepta	1.03	0.00048354	0.265
M-nona	0.9	0.000325	0.576	M-nona	0.98	0.00032352	0.641
<i>T. chumash</i>				<i>T. cristinae</i>			
CHC	X-fold	Observed	P-value	CHC	X-fold	Observed	P-value
F-penta	0.89	0.00036706	0.983	F-penta	1.01	0.00041936	0.217
F-hepta	0.94	0.00027501	0.898	F-hepta	1.01	0.00029503	0.266
F-nona	0.98	0.00025862	0.674	F-nona	0.94	0.00024953	0.997
M-penta	0.99	0.00035754	0.512	M-penta	0.99	0.0003586	0.509
M-hepta	0.97	0.00045792	0.712	M-hepta	0.95	0.00044654	0.992
M-nona	1.06	0.00034639	0.122	M-nona	0.97	0.00031857	0.942
<i>T. knulli</i>				<i>T. poppensis</i>			
CHC	X-fold	Observed	P-value	CHC	X-fold	Observed	P-value
F-penta	0.96	0.00039798	0.859	F-penta	0.98	0.00040417	0.689
F-hepta	1.02	0.00029934	0.201	F-hepta	0.99	0.00029192	0.521
F-nona	1.03	0.00027378	0.132	F-nona	0.96	0.00025463	0.856
M-penta	1.02	0.00036701	0.232	M-penta	1	0.00036056	0.429
M-hepta	0.99	0.00046794	0.554	M-hepta	1.03	0.00048384	0.208
M-nona	1	0.00033049	0.465	M-nona	1.07	0.00035128	0.024
<i>T. landelsensis</i>				<i>T. californicum</i>			
CHC	X-fold	Observed	P-value	CHC	X-fold	Observed	P-value
F-penta	0.94	0.00039035	0.951	F-penta	0.97	0.00040217	0.753
F-hepta	0.98	0.00028747	0.684	F-hepta	0.99	0.00028878	0.601
F-nona	0.97	0.00025692	0.819	F-nona	0.98	0.00026206	0.625
M-penta	0.98	0.00035169	0.726	M-penta	0.96	0.00034453	0.892
M-hepta	1.03	0.00048427	0.201	M-hepta	1.05	0.00049524	0.071
M-nona	1.02	0.00033471	0.304	M-nona	1.01	0.00033312	0.333

1027

1028 Table S7: X-fold enrichments and associated *P*-values for number of overlapping SNP windows
 1029 for PC2 for comparison with CHC experiment. Observed value gives the mean posterior
 1030 inclusions probability (i.e., probability of a genotype-phenotype association) across all SNPs in
 1031 100 kb windows for each of the six CHC traits. *P*-values $\leq .05$ are highlighted in bold.

<i>T. bartmani</i>				<i>T. podura</i>			
CHC	X-fold	Observed	P-value	CHC	X-fold	Observed	P-value
F-penta	0.97	0.000403	0.681	F-penta	0.99	0.00041351	0.486
F-hepta	1.05	0.000306	0.143	F-hepta	0.92	0.00027053	0.978
F-nona	1	0.000265	0.494	F-nona	1.06	0.00028006	0.089
M-penta	0.96	0.000345	0.773	M-penta	0.97	0.00035019	0.709
M-hepta	0.96	0.000455	0.734	M-hepta	1.05	0.00049492	0.113
M-nona	0.99	0.000326	0.573	M-nona	0.89	0.0002953	0.994
<i>T. chumash</i>				<i>T. cristinae</i>			
CHC	X-fold	Observed	P-value	CHC	X-fold	Observed	P-value
F-penta	1.01	0.00041693	0.417	F-penta	1.05	0.0004352	0.009
F-hepta	0.95	0.00027777	0.863	F-hepta	0.98	0.00028726	0.805
F-nona	1.04	0.00027621	0.191	F-nona	1.01	0.00026784	0.286
M-penta	1.05	0.00037559	0.172	M-penta	1.01	0.00036299	0.286
M-hepta	0.98	0.00046092	0.628	M-hepta	0.96	0.00045164	0.976
M-nona	0.92	0.00030343	0.955	M-nona	0.99	0.00032555	0.681
<i>T. knulli</i>				<i>T. poppensis</i>			
CHC	X-fold	Observed	P-value	CHC	X-fold	Observed	P-value
F-penta	1.02	0.00041785	0.295	F-penta	1.03	0.00042699	0.171
F-hepta	1.02	0.00029805	0.221	F-hepta	1.04	0.0003051	0.087
F-nona	0.98	0.00025978	0.738	F-nona	0.97	0.00025664	0.811
M-penta	0.97	0.00034943	0.806	M-penta	1.06	0.0003824	0.042
M-hepta	0.99	0.00046472	0.612	M-hepta	1.05	0.00049262	0.093
M-nona	1	0.00032921	0.471	M-nona	0.97	0.00032084	0.772
<i>T. landelsensis</i>				<i>T. californicum</i>			
CHC	X-fold	Observed	P-value	CHC	X-fold	Observed	P-value
F-penta	0.92	0.00038096	0.987	F-penta	0.95	0.00039456	0.895
F-hepta	0.97	0.0002817	0.864	F-hepta	0.93	0.00027181	0.99
F-nona	1.01	0.00026628	0.43	F-nona	1.01	0.00026813	0.346
M-penta	0.99	0.00035724	0.517	M-penta	1.05	0.00037699	0.062
M-hepta	1.01	0.00047379	0.437	M-hepta	1.01	0.00047356	0.395
M-nona	0.99	0.00032686	0.561	M-nona	0.96	0.00031934	0.831

1032 Table S8: X-fold enrichments and associated *P*-values for number of overlapping SNP windows
 1033 for PC3 for comparison with CHC experiment. Observed value gives the mean posterior
 1034 inclusions probability (i.e., probability of a genotype-phenotype association) across all SNPs in
 1035 100 kb windows for each of the six CHC traits. *P*-values $\leq .05$ are highlighted in bold.

<i>T. bartmani</i>				<i>T. podura</i>			
CHC	X-fold	Observed	P-value	CHC	X-fold	Observed	P-value
F-penta	1.06	0.000439	0.128	F-penta	1.03	0.00042715	0.222
F-hepta	1.02	0.000301	0.271	F-hepta	1.04	0.00030464	0.132
F-nona	0.99	0.000264	0.526	F-nona	0.93	0.00024736	0.948
M-penta	0.96	0.000345	0.781	M-penta	1.08	0.00038877	0.029
M-hepta	1.07	0.000508	0.072	M-hepta	1.09	0.00051268	0.028
M-nona	0.9	0.000325	0.576	M-nona	0.99	0.00032619	0.531
<i>T. Chumash</i>				<i>T. cristinae</i>			
CHC	X-fold	Observed	P-value	CHC	X-fold	Observed	P-value
F-penta	1.07	0.0004442	0.088	F-penta	1.05	0.00043482	0.012
F-hepta	0.99	0.0002889	0.569	F-hepta	1.01	0.00029312	0.393
F-nona	0.94	0.00024939	0.889	F-nona	1.03	0.00027351	0.051
M-penta	1.03	0.00037132	0.216	M-penta	0.99	0.00035579	0.666
M-hepta	1.03	0.00048255	0.281	M-hepta	0.98	0.00046005	0.832
M-nona	1.05	0.00034602	0.164	M-nona	0.98	0.00032394	0.791
<i>T. knulli</i>				<i>T. poppensis</i>			
CHC	X-fold	Observed	P-value	CHC	X-fold	Observed	P-value
F-penta	1.05	0.00043564	0.054	F-penta	1.06	0.00043928	0.034
F-hepta	0.99	0.0002911	0.547	F-hepta	0.97	0.00028301	0.832
F-nona	0.97	0.00025644	0.842	F-nona	0.96	0.00025389	0.894
M-penta	1.03	0.00036955	0.141	M-penta	0.93	0.00033533	0.981
M-hepta	0.99	0.00046841	0.563	M-hepta	0.98	0.0004604	0.723
M-nona	0.99	0.00032395	0.676	M-nona	0.96	0.00031526	0.903
<i>T. landelsensis</i>				<i>T. californicum</i>			
CHC	X-fold	Observed	P-value	CHC	X-fold	Observed	P-value
F-penta	1.03	0.0004247	0.236	F-penta	1.02	0.0004232	0.268
F-hepta	1.03	0.00030062	0.175	F-hepta	0.95	0.00027931	0.913
F-nona	0.99	0.00026403	0.532	F-nona	0.97	0.00026	0.732
M-penta	0.97	0.00034978	0.769	M-penta	0.98	0.00035164	0.713
M-hepta	0.95	0.00044452	0.939	M-hepta	1.05	0.00049509	0.068
M-nona	1.05	0.00034642	0.056	M-nona	0.99	0.00032631	0.594

1036

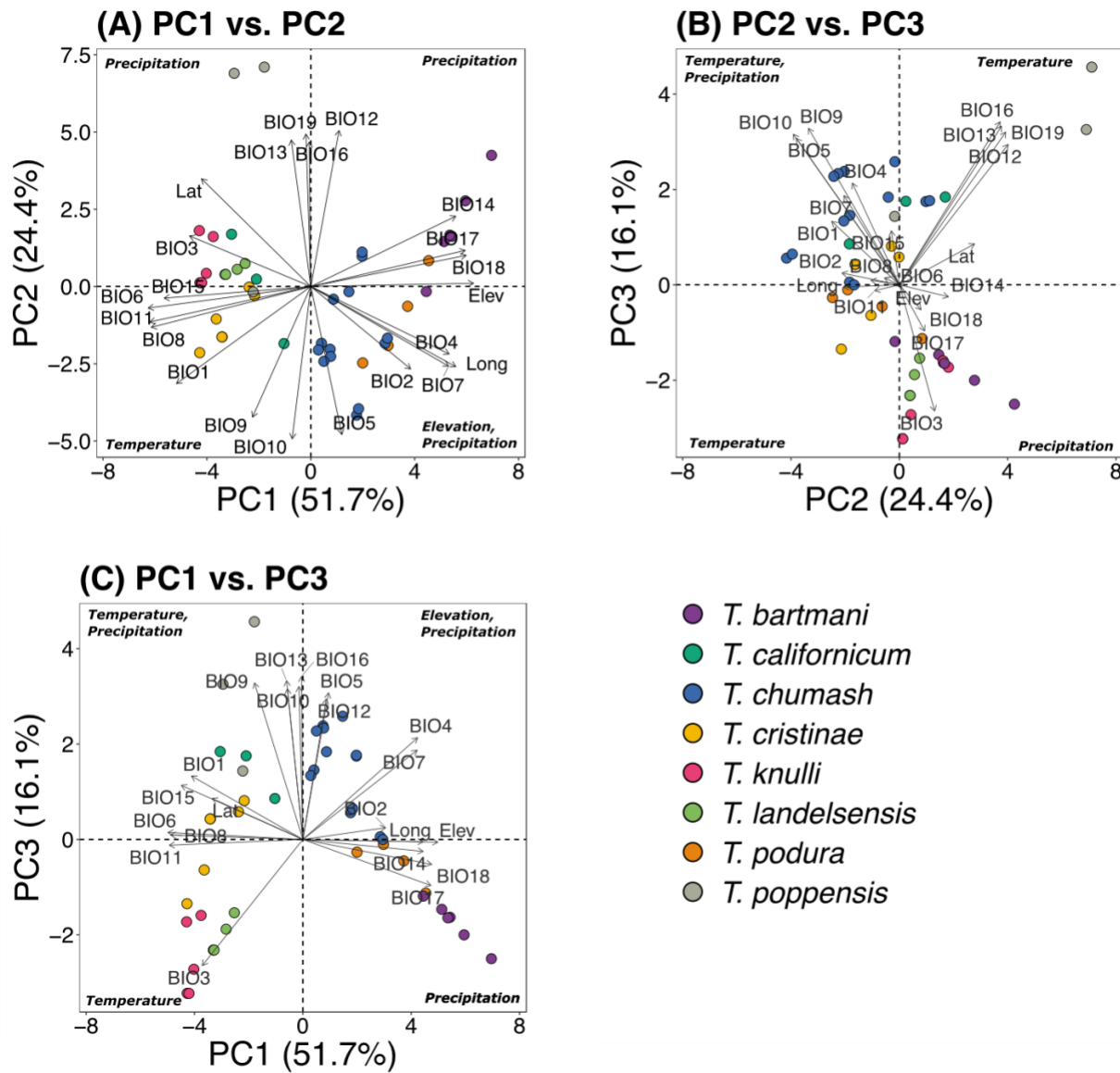
1037 Table S9: Proportion of variation explained by the TREEMIX population graph with different
1038 numbers of migration edges.

Number of migration edges	Proportion of variation explained
0	0.997
1	0.998
2	0.998
3	0.998
4	0.999
5	0.999
6	0.999
7	0.999
8	0.999
9	0.999

1039

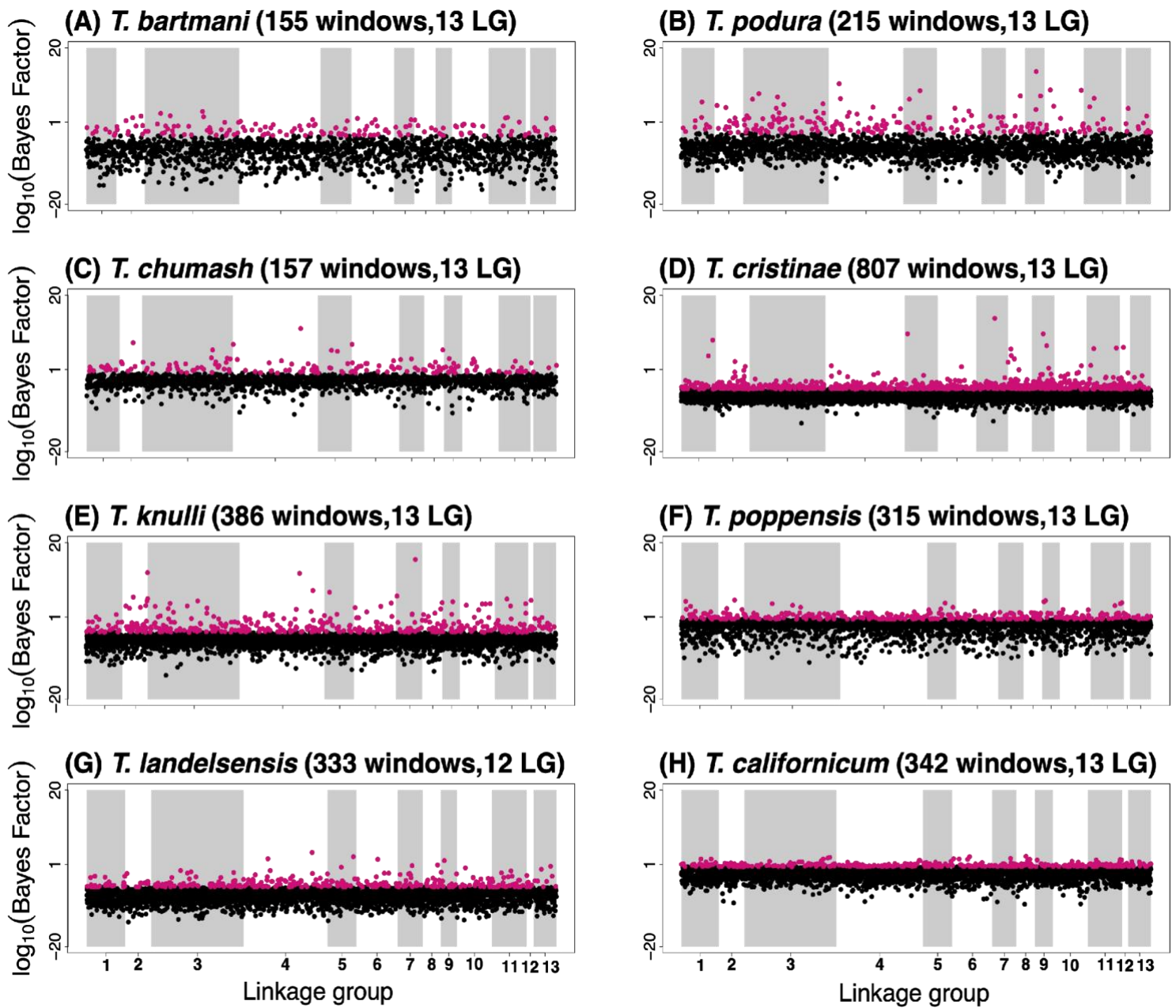
1040 **SUPPLEMENTARY FIGURES**

1041 Figure S1: Ordination of climate variation (22 variables, see Table S2 for code descriptions) via
 1042 principal component analysis (PCA). Points denote the study populations, colour-coded by
 1043 species.



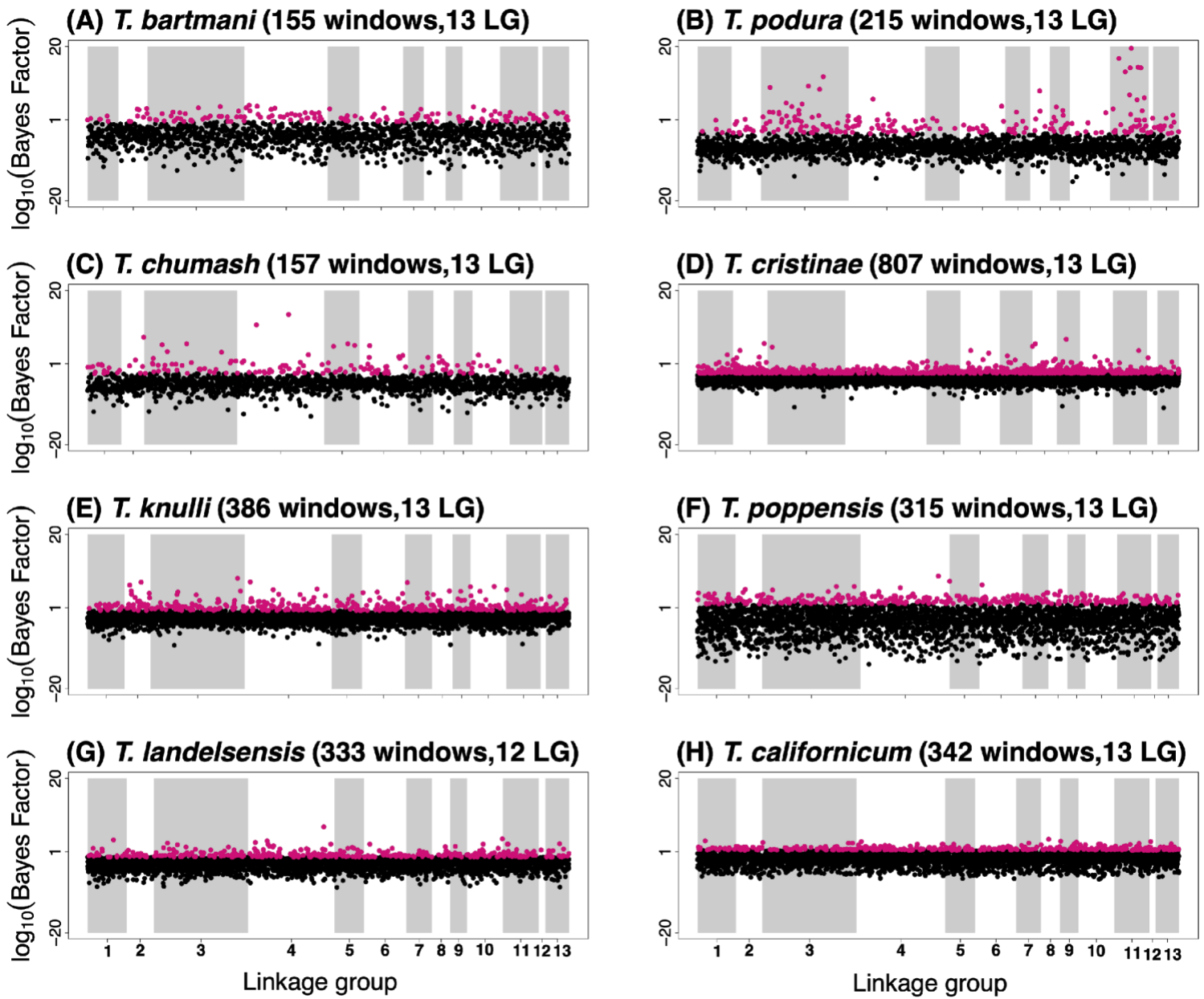
1044

1045 Figure S2: Manhattan plots showing the strength of evidence for association (measured here
 1046 using the Bayes factor from the software BayPass) between a SNP window and climate for PC1.
 1047 Results are shown along the 13 linkage groups. Red points denote the SNP windows in the top
 1048 10% quantile (i.e., referred to as 'climate-associated SNP windows' throughout the main text). In
 1049 each panel title, the two values in parentheses are the number of SNP windows in the top 10%
 1050 quantile ("windows"), followed by the number of linkage groups with at least 1 SNP window in
 1051 the top 10% quantile ("LG").



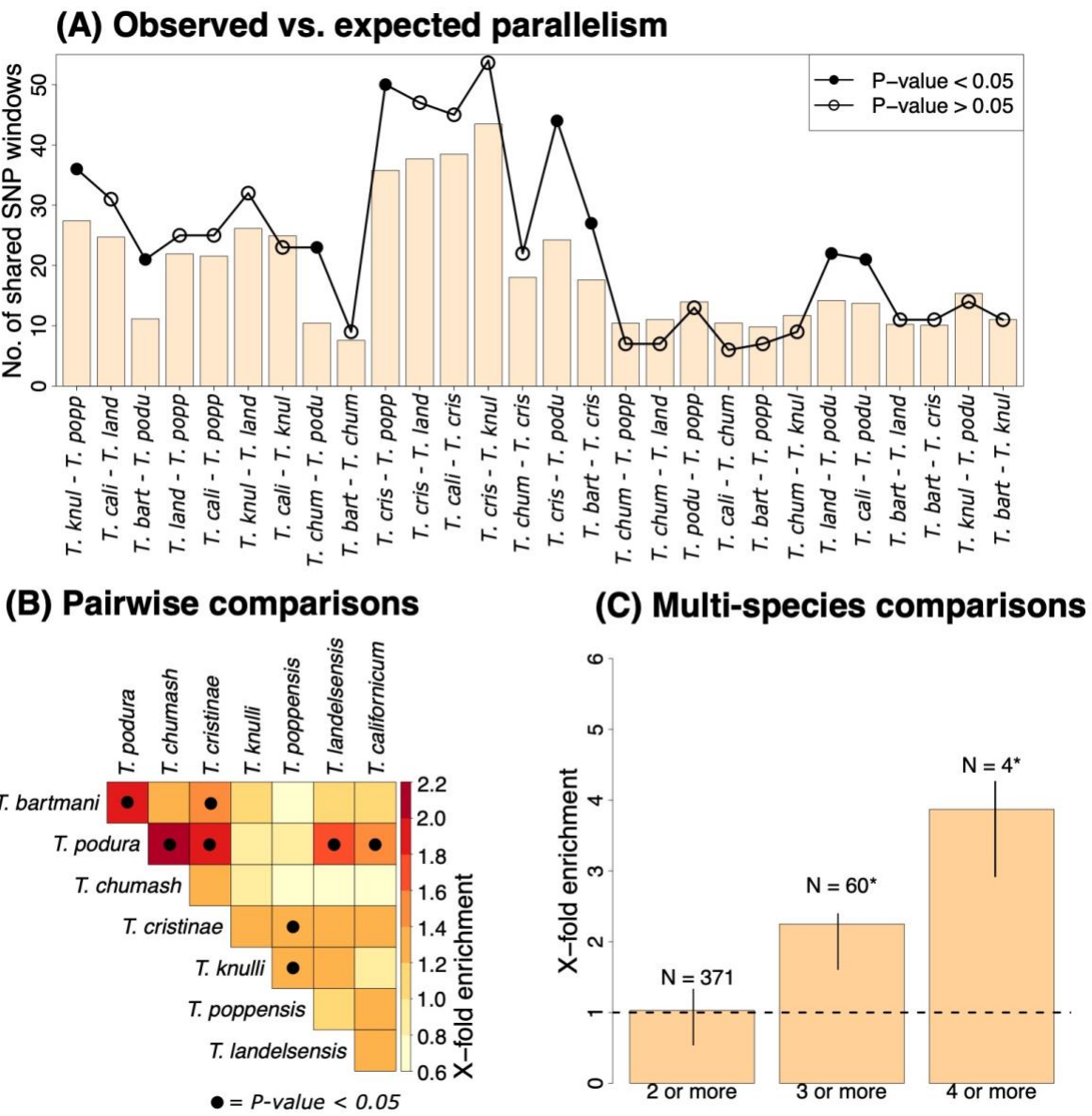
1052

1053 Figure S3: Manhattan plots showing the strength of evidence for association (measured here
 1054 using the Bayes factor from the software BayPass) between a SNP window and climate for PC2.
 1055 Results are shown along the 13 linkage groups. Red points denote the SNP windows in the top
 1056 10% quantile (i.e., referred to as 'climate-associated SNP windows' throughout the main text). In
 1057 each panel title, the two values in parentheses are the number of SNP windows in the top 10%
 1058 quantile ("windows"), followed by the number of linkage groups with at least 1 SNP window in
 1059 the top 10% quantile ("LG").



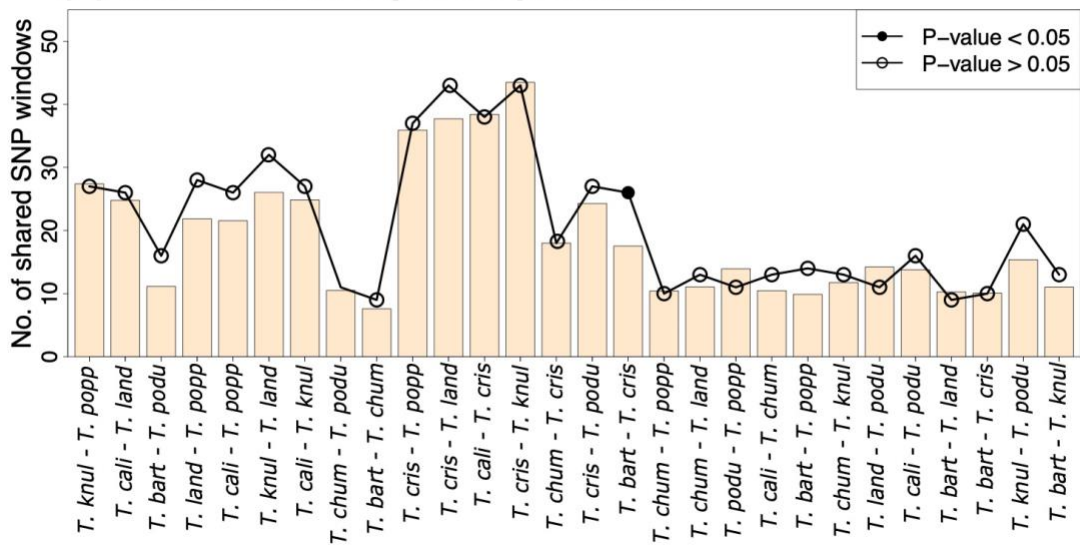
1060

1061 FIGURE S4: Tests for parallel climate-associated SNP windows between and among species of
 1062 *Timema* stick insects (all plots are for the top 10% empirical quantile) for PC1. (A) Plot shows
 1063 observed versus expected number of overlapping climate-associated SNP windows for species
 1064 pairwise comparison for PC1. Bars denote expected values and dotted lines denotes observed
 1065 values. Open points indicate P-value > 0.05 and filled points indicate P-value ≤ 0.05. (B)
 1066 Pairwise plot shows x-fold enrichment values for each comparison between pairs of species.
 1067 Black dot on each box denotes P-value ≤ 0.05. (C) Plot shows x-fold enrichments for number of
 1068 overlapping climate-associated SNP windows for PC1 for comparisons between multiple
 1069 species, i.e., beyond pairs of species (e.g., 2 or more species, 3 or more species, 4 or more
 1070 species). Bars denote observed x-fold value for each multi-species comparison. Black lines on
 1071 bars show the 95% confidence intervals. N value above each bar indicates the observed number
 1072 of overlapping climate-associated SNP windows for each comparison. * Indicates x-fold
 1073 enrichments with P-value ≤ 0.05.

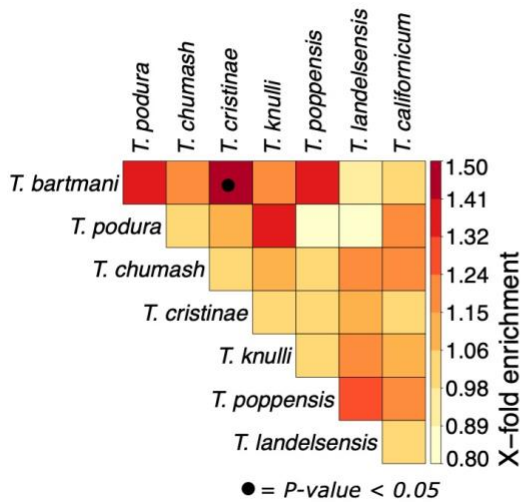


1075 FIGURE S5: Tests for parallel climate-associated SNP windows between and among species of
 1076 *Timema* stick insects (all plots are for the top 10% empirical quantile) for PC2. (A) Plot shows
 1077 observed versus expected number of overlapping climate-associated SNP windows for species
 1078 pairwise comparison for PC2. Bars denote expected values and dotted lines denotes observed
 1079 values. Open points indicate P-value > 0.05 and filled points indicate P-value ≤ 0.05. (B)
 1080 Pairwise plot shows x-fold enrichment values for each comparison between pairs of species.
 1081 Black dot on each box denotes P-value ≤ 0.05. (C) Plot shows x-fold enrichments for number of
 1082 overlapping climate-associated SNP windows for PC2 for comparisons between multiple
 1083 species, i.e., beyond pairs of species (e.g., 2 or more species, 3 or more species, 4 or more
 1084 species). Bars denote observed x-fold value for each multi-species comparison. Black lines on
 1085 bars show the 95% confidence intervals. N value above each bar indicates the observed number
 1086 of overlapping climate-associated SNP windows for each comparison. * Indicates x-fold
 1087 enrichments with P-value ≤ 0.05.

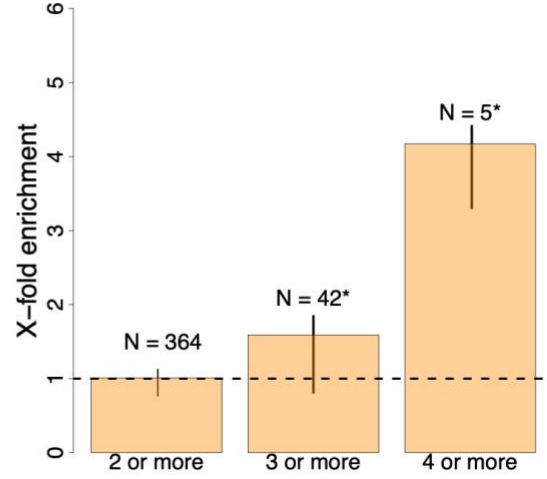
(A) Observed vs. expected parallelism



(B) Pairwise comparisons

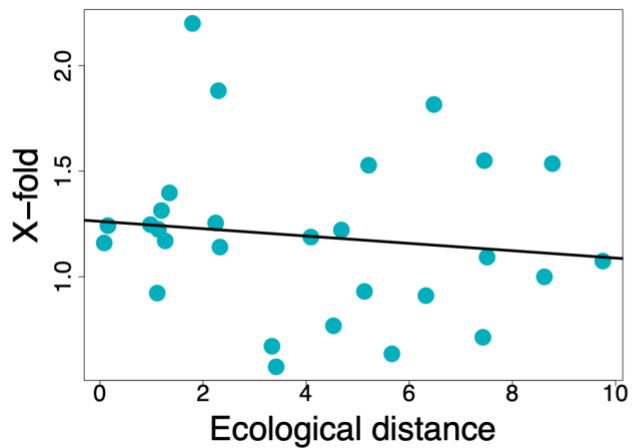


(C) Multi-species comparisons

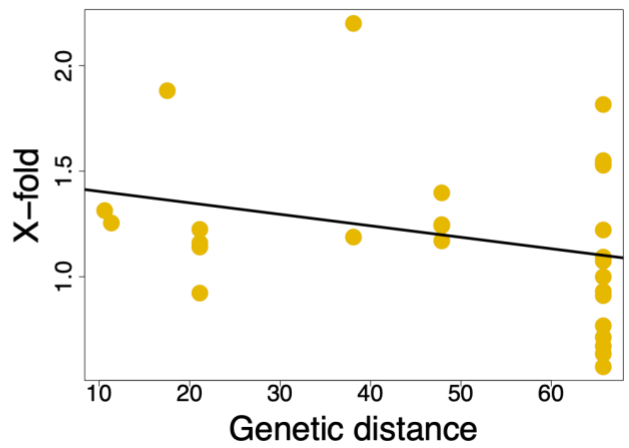


1089 FIGURE S6: Test results of the “shared ecology” versus “shared genetics” hypotheses. (A)
 1090 Scatterplot shows the relationship between X-fold enrichment (measure for parallelism) and
 1091 ecological distance (measured as distance in PC1 scores) (B) Scatterplot shows the relationship
 1092 between X-fold enrichment (measure for parallelism) and genetic distance (measured as pairwise
 1093 phylogenetic distance). (C) Scatterplot shows the relationship between ecological distance
 1094 (measured as distance in PC1 scores and is distance in climate variables) and genetic distance
 1095 (measured as pairwise phylogenetic distance) (D) Plot shows parameter estimates with
 1096 standardized coefficients for the full model for PC1. A negative or positive estimate which
 1097 deviates from zero is indicative of effect on parallelism.

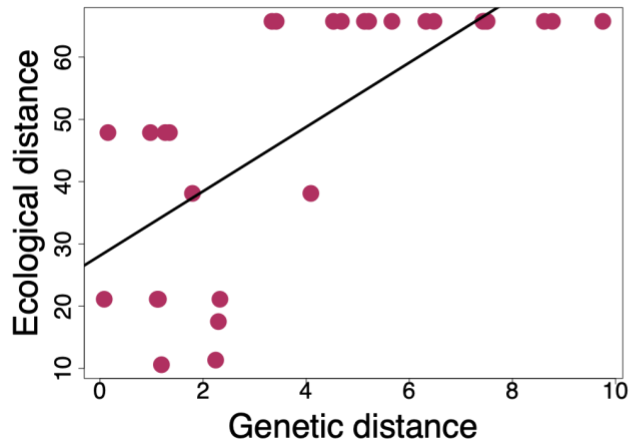
(A) Parallelism vs. ecological distance



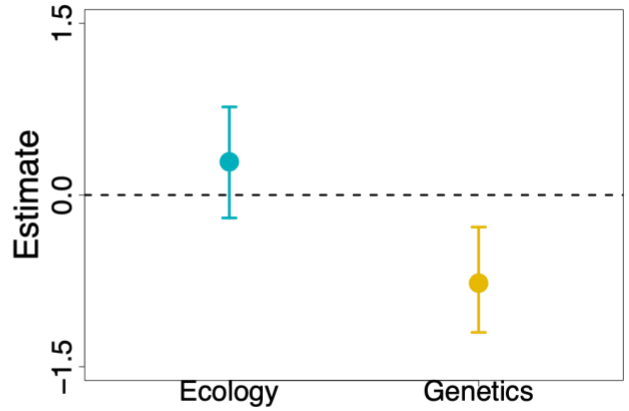
(B) Parallelism vs. genetic distance



(C) Ecological distance vs. genetic distance



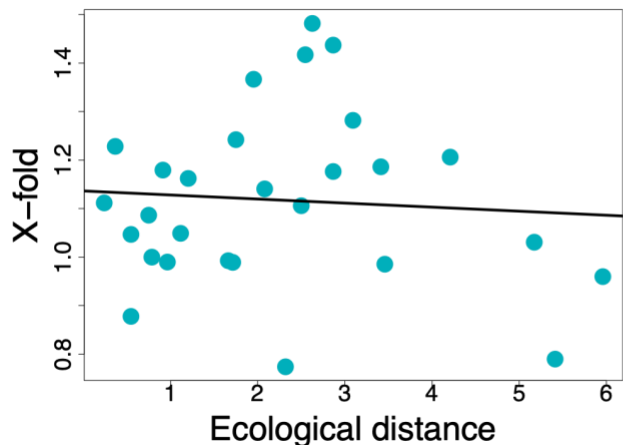
(D) Ecology vs. genetics (model)



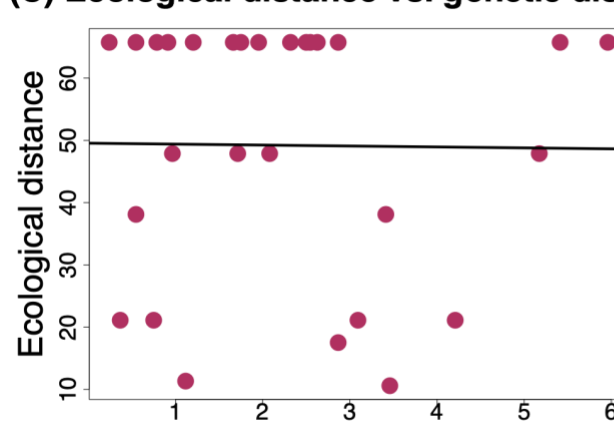
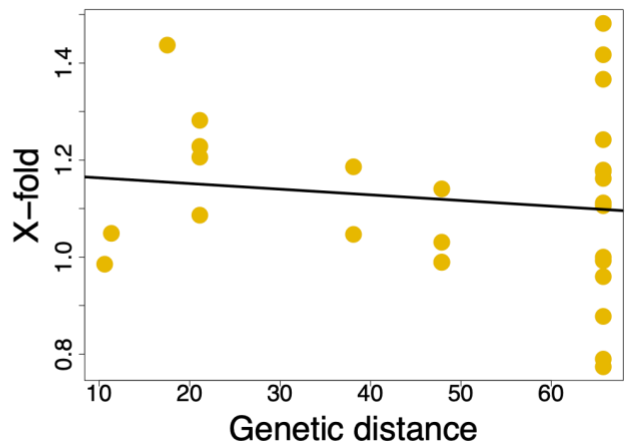
1098

1099 FIGURE S7: Test results of the “shared ecology” versus “shared genetics” hypotheses. (A)
 1100 Scatterplot shows the relationship between X-fold enrichment (measure for parallelism) and
 1101 ecological distance (measured as distance in PC2 scores) (B) Scatterplot shows the relationship
 1102 between X-fold enrichment (measure for parallelism) and genetic distance (measured as pairwise
 1103 phylogenetic distance). (C) Scatterplot shows the relationship between ecological distance
 1104 (measured as distance in PC2 scores and is distance in climate variables) and genetic distance
 1105 (measured as pairwise phylogenetic distance) (D) Plot shows parameter estimates with
 1106 standardized coefficients for the full model only for PC2. A negative or positive estimate which
 1107 deviates from zero is indicative of effect on parallelism.

(A) Parallelism vs. ecological distance



(B) Parallelism vs. genetic distance



1109 FIGURE S8, S9, S10: Plots show summaries of population structure based on principal
1110 component analysis for 8 species included in this study for PC1 vs. PC2 (Figure 19), PC1 vs.
1111 PC3 (Figure 20), and PC2 vs. PC3 (Figure21). Abbreviations indicate populations corresponding
1112 to TABLE S1.

